

**A Study on the Network Microdomain Structure  
in Block Copolymer Melts**

Wang Yi-Chin

2016



# Contents

## Chapter 1. General Introduction

<b>1-1. The Physics of Block Copolymer</b> .....	<b>1</b>
1-1-1. Introduction .....	1
<b>1-2. Introduction to Diblock Copolymer Melts</b> .....	<b>4</b>
1-2-1. Order-Disorder Transition of Diblock Copolymer Melts .....	4
1-2-2. Phase Behaviors of Diblock Copolymer Melts .....	6
<b>1-3. Multiblock Copolymer Systems: Triblock Copolymer Melts</b> .....	<b>9</b>
1-3-1. Introduction to Multiblock Copolymer Melts .....	9
1-3-2. Order-Disorder Transition of Triblock Copolymer Melts .....	10
1-3-3. Morphological behavior of ABC Triblock Copolymer Melts .....	11
<b>1-4. Ordered Network Morphology in Block Copolymer Melts</b> .....	<b>15</b>
1-4-1. Introduction to Network Morphologies .....	15
1-4-2. Ordered Bicontinuous Double-Diamond Morphology .....	17
1-4-3. Double Gyroid Network Morphology .....	18
1-4-4. Orthorhombic <i>Fddd</i> Network Morphology .....	19
1-4-5. Orthorhombic <i>Pnna</i> Network Morphology .....	20
<b>1-5. Structural Analysis</b> .....	<b>21</b>
1-5-1. Small-Angle X-ray Scattering .....	21

1-5-2. Electron Tomography .....	23
<b>1-6. Contents of this thesis .....</b>	<b>25</b>
<b>Reference .....</b>	<b>28</b>

## **Chapter 2. Orthorhombic *Fddd* Microdomain Structure in Diblock Copolymer**

<b>2-1. Introduction .....</b>	<b>35</b>
<b>2-2. Experimental Section .....</b>	<b>37</b>
<b>2-3. Results and Discussion .....</b>	<b>39</b>
<b>2-4. Conclusions .....</b>	<b>50</b>
<b>Reference .....</b>	<b>52</b>

## **Chapter 3. *Fddd* Structure in Polystyrene-*block*-polyisoprene Diblock Copolymer/ Polystyrene Homopolymer Blends**

<b>3-1. Introduction .....</b>	<b>55</b>
<b>3-2. Experimental Section .....</b>	<b>56</b>
<b>3-3. Results and Discussion .....</b>	<b>58</b>
<b>3-4. Conclusions .....</b>	<b>66</b>
<b>Reference .....</b>	<b>67</b>

## **Chapter 4. 3D-TEM Study on the Morphology of PS-*b*-(PVPDVS-*g*-PI)**

### **Block-Graft Copolymer**

<b>4-1. Introduction</b> .....	<b>69</b>
<b>4-2. Experimental Section</b> .....	<b>71</b>
<b>4-3. Results and Discussion</b> .....	<b>73</b>
<b>4-4. Conclusions</b> .....	<b>81</b>
<b>Reference</b> .....	<b>82</b>

## **Chapter 5. The formation of OBDD Network Structure in**

### **PS-*b*-PI-*b*-PDMS Triblock Copolymer**

<b>5-1. Introduction</b> .....	<b>83</b>
<b>5-2. Experimental Section</b> .....	<b>85</b>
<b>5-3. Results and Discussion</b> .....	<b>88</b>
<b>5-4. Conclusions</b> .....	<b>99</b>
<b>Reference</b> .....	<b>100</b>

## **Chapter 6. Morphological Control in PS-*b*-PI-*b*-PDMS Triblock**

### **Copolymer by Mixed-Solvent**

<b>6-1. Introduction</b> .....	<b>103</b>
<b>6-2. Experimental Section</b> .....	<b>105</b>
<b>6-3. Results and Discussion</b> .....	<b>108</b>
6-3-1. Equilibrium Structure of SID2 Triblock Copolymer .....	108
6-3-2. Morphology of SID2 Film Cast from Toluene Solution .....	109
6-3-3. Morphology of SID2 Solutions with Different Weight Ratio in Mixed-Solvent .....	111
6-3-4. Preservation of Morphologies of Solution State .....	113
<b>6-4. Conclusions</b> .....	<b>115</b>
<b>Reference</b> .....	<b>116</b>
<b>Summary</b> .....	<b>117</b>
<b>List of Publications</b> .....	<b>121</b>
<b>Acknowledgment</b> .....	<b>123</b>

# *Chapter 1*

## **General Introduction**

### **1-1. The Physics of Block Copolymer**

#### **1-1-1. Introduction**

Block copolymers, which are known as soft materials, are defined as the polymers composed of two or more kinds of chemically different polymers chains connected by a covalent bond. Since Szwarc firstly synthesized a block copolymer by using living anionic polymerization technique<sup>1</sup>, a variety of block copolymers such as triblock, multiblock, and starblock copolymers have been synthesized as shown in Figure 1-1. The recent development of living cationic polymerization<sup>2</sup> and living radical polymerization<sup>3</sup> techniques has increased the numbers of accessible monomers and expanded the field of the applications of block copolymers.

The control of phase behaviors and morphologies of block copolymer is important for us to apply the block copolymers to practical applications such as microporous membrane, optical film and so on. We thus need to clarify the mechanism of the self-assembly of block copolymers. The clarification would contribute to the progress in soft material physics.

In this thesis, I focus on the self-assembly of network morphologies in block copolymers. Various network microdomain morphologies have been revealed and has stimulated this thesis to investigate these network morphologies more deeply. Moreover, self-assembly of the periodic network structures depends on various parameters: volume fraction, molecular weight, temperature, and is affected by the formation process such as solvent cast, melt press, shear, and so on. To clarify the relationship between morphologies and parameters and processes is an important issue to better control and create complex microdomain morphologies. Hence I aimed to study and control the block copolymers that form 3D periodic continuous network morphologies.

In this chapter, the overview of block copolymer physics will be presented as Introduction of this thesis. Firstly, the order-disorder transition and morphologies in diblock copolymer melts will be described. Then, the discussion for diblock copolymer melts will be expanded to the case of triblock copolymer melts. Secondary, the features of the network structures in block copolymers will be described. Finally, the techniques of structural analysis used in the thesis will be presented.

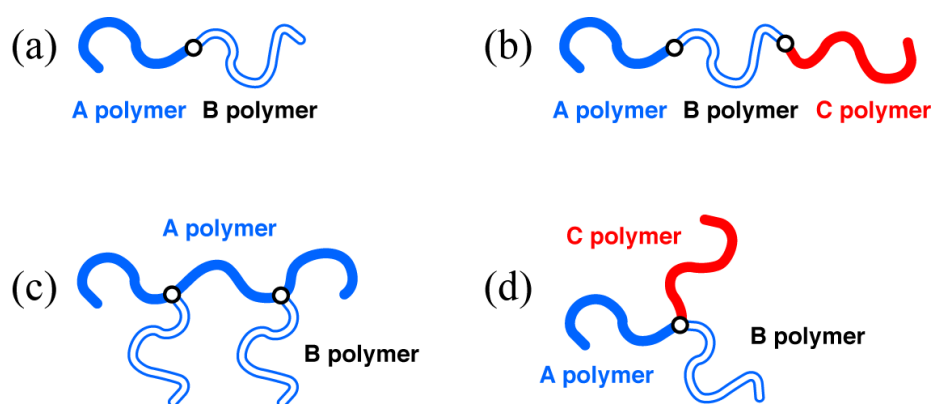


**Figure 1-1.** Schematic illustrations of block copolymers: (a) AB diblock copolymer, (b) ABC linear triblock copolymer, (c) (AB)A(AB)  $\pi$ -shaped graft copolymer, (d) ABC star triblock copolymer.

## 1-2. Introduction to Diblock Copolymer Melts

### 1-2-1. Order-Disorder Transition of Diblock Copolymer Melts

Here the order-disorder transition of the simplest AB diblock copolymer melts is discussed. The order-disorder transition is the thermodynamic phase transition, and is dictated by the competition between the entropy and the enthalpy. The entropic term is inversely proportional to the total number of monomers  $N$  per polymer chain of the diblock copolymer ( $N = N_A + N_B$ ), where  $N_i$  is the total number of monomers in  $i$ -th component chain. The term  $\chi_{AB}N$  is used to express the energy cost for mixing two species homogeneously, where  $\chi_{AB}$  is the segment-segment interaction parameter between two block chains. When  $\chi_{AB}N$  is smaller than the critical value,  $(\chi_{AB}N)_{ODT}$ , A and B chains are mixed in the molecular level as shown in Figure 1-2 (a) and this homogeneous state is defined as disordered state. In contrast, when  $\chi_{AB}N > (\chi_{AB}N)_{ODT}$ , A and B block chains segregate into A and B rich phases, respectively, and result in a periodic microdomain structure with long-range order (Figure 1-2 (b)). The transition is called the order-disorder transition.

Since the chemical junctions connect A and B block chains at the interface between two microdomains, the size of the phase separation is limited to the radius of the gyration of block copolymer ( $R_g \sim 5 - 100$  nm), and thus the phase separation is called microphase separation. The following typical equilibrium microphase morphologies can be formed by microphase separation as shown in Figure 1-2 (c): spheres in the body-centered cubic lattice (BCC), hexagonally-packed cylinders (HEX),

double gyroid ( $Ia\bar{3}d$ ), lamellae (LAM) <sup>4, 5</sup>. Recently,  $Fddd$  has been found as a fifth equilibrium morphology between LAM and  $Ia\bar{3}d$  phases<sup>6-10</sup>.

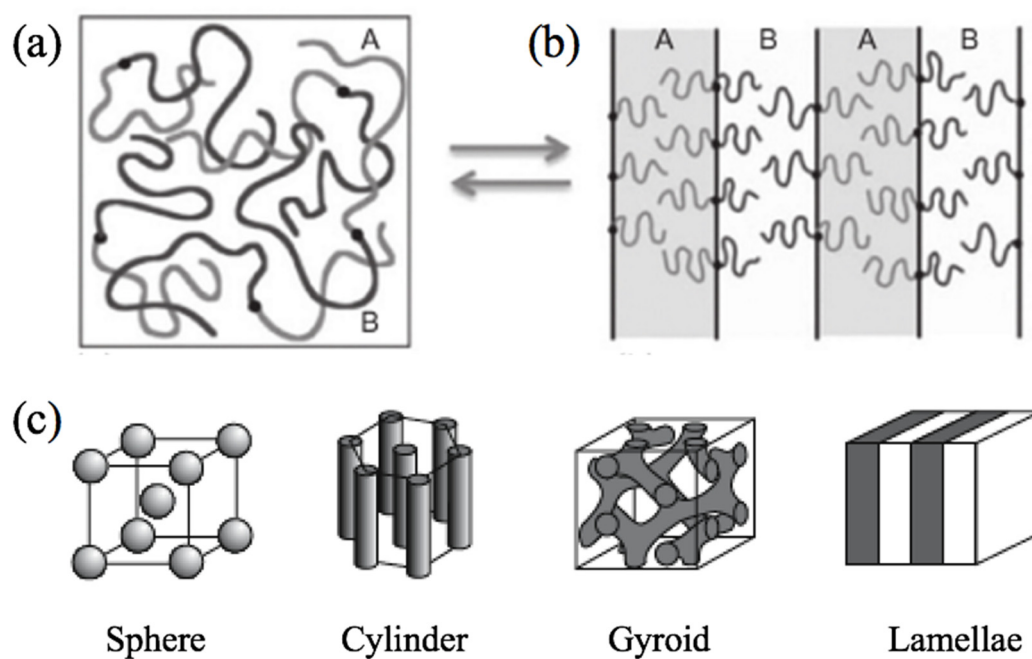


**Figure 1-2.** Schematic illustrations of (a) disordered state, (b) ordered state of AB diblock copolymer. (c) Typical thermodynamically stable morphologies in AB diblock copolymer.

### 1-2-2. Phase Behaviors of Diblock Copolymer Melts

The phase behaviors of block copolymer melts can be theoretically described by various approaches<sup>11, 12</sup>. Leibler investigated the phase behaviors of diblock copolymer melts by using Ginzburg-Landau (GL) free energy function. He estimated the critical value  $(\chi_{AB}N)_{ODT}$  as 10.5 for diblock copolymer melts, and determined their phase behaviors. Near  $f = 0.5$ , LAM is thermodynamically stable and it changes to HEX and finally to BCC as  $f$  becomes asymmetric. Later gyroid structure has been found to locate between the LAM and HEX phase by GL free energy function by Podnec and Hamley<sup>13</sup>. From the view point of the physics of block copolymer, Leibler's theory agrees with the experimental result qualitatively. However, though the theory predicts the order-order transition in the order of BCC, HEX, and LAM near  $f = 0.5$ , the direct transition from disorder to HEX near  $f = 0.5$  is observed experimentally. Fredrickson and Helfand suggested that this difference is caused by the effects of thermal fluctuations, and calculated the phase behaviors with the effects. The calculated results predicted the expansion of the disordered state to  $\chi_{AB}N > 10.5$  and the direct phase transitions from disordered to LAM, HEX and  $Ia\bar{3}d$  are predicted at asymmetric volume fraction.

Matsen and Schick examined the phase diagram of diblock copolymer from the weak segregation limit (WSL) to the strong segregation limit (SSL) by using self-consistent field theory (SCFT) and six ordered morphologies: LAM,  $Fddd$ ,  $Ia\bar{3}d$ , HEX, BCC, and CPS has found to be thermodynamically stable as shown in Figure 1-3

(a)<sup>4</sup>. The experimental results of polystyrene-*block*-polyisoprene (SI) obtained by Khandpur et al.<sup>14</sup> is shown in Figure 1-3 (b). LAM phase is found at  $f = 0.5$ , and as volume fraction  $f$  is biased,  $Ia\bar{3}d$ , HEX and BCC phases are observed.

According to Figure 1-3, some disagreements between phase diagram calculated by SCFT and the experimental results exist even though experimental results agree with SCFT prediction. Firstly, effects of the thermal fluctuations are not included in the SCFT calculation, and thus the stable phases in the order of disordered, BCC, HEX and to LAM near  $f = 0.5$  with increasing  $\chi_{AB}N$ . However, the order-disorder transition point around  $\chi_{AB}N = 20$  is observed in the experiments. Also, direct phase transitions are allowed from disordered to LAM, HEX, and  $Ia\bar{3}d$  phases in experiments. Secondary, the phase diagram determined by experiments is asymmetric, which originates from the asymmetry in statistical segment length and monomer volume between PS and PI blocks<sup>15</sup>.

Recently, a new equilibrium bicontinuous microdomain morphology with the symmetry of  $Fddd$  space group has been found in polystyrene-*block*-polyisoprene (SI) diblock copolymer, and located between LAM and  $Ia\bar{3}d$  phase in the phase diagram of block copolymer<sup>6, 8</sup>.

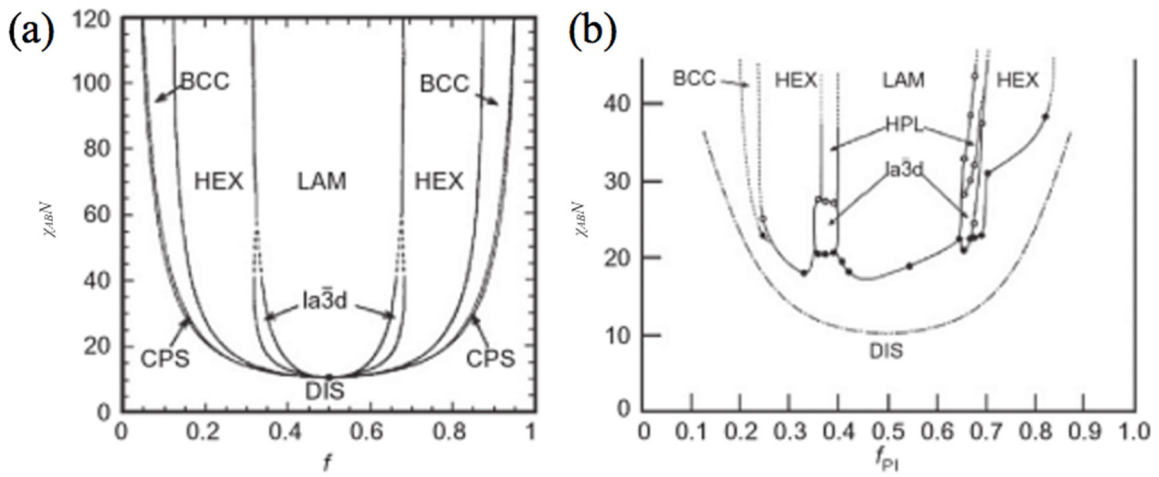


**Figure 1-3.** Phase diagram of (a) theoretical calculation with self-consistent field theory by Masten<sup>4</sup>, and (b) experimental results of polystyrene-*block*-polyisoprene (SI) by Khandpur et al<sup>14</sup>.

## 1-3. Multiblock Copolymer Systems: Triblock Copolymer Melts

### 1-3-1. Introduction to Multiblock Copolymer Melts

Development in anionic polymerization techniques enabled us to achieve the well-defined block copolymers consist of more than two different blocks<sup>16-19</sup>. Studies of morphological behaviors in multiblock copolymers such as linear ABC triblock terpolymers<sup>12, 20-26</sup> and linear ABCD tetrablock quaterpolymers<sup>25, 27</sup> have been reported.

ABC triblock copolymers consist of mutually immiscible A, B, and C polymer segments that are bonded together chemically, they also undergo microphase separation and form three independent microphases as diblock copolymer do. The addition of C component increases the number of parameters controlling the phase behaviors in ABC triblock copolymers. The parameters for the ABC triblock copolymer are the following seven quantities controlling their phase behaviors: two volume fractions  $\Phi_A$ ,  $\Phi_B$ ; three interaction parameters  $\chi_{AB}$ ,  $\chi_{BC}$ ,  $\chi_{CA}$ ; and two relative segment lengths  $a_B/a_A$ ,  $a_C/a_A$ , while there are only three quantities for diblock copolymers:  $\Phi_A$ ,  $\chi_{AB}$  and  $a_B/a_A$ .

Moreover, the sequence of blocks in the linear chain (chain topology) is important in triblock copolymers. Thermodynamic properties and the microphase morphological transition of A-B-C, B-A-C, and C-A-B triblock copolymers are expected to be significantly different. According to the theoretical study, attaching C block to one end of AB diblock copolymer would alter the repulsive interaction between A and B block<sup>28</sup>.

### 1-3-2. Order-Disorder Transition of Triblock Copolymer Melts

Pronounced influence of the block sequence on the ODT was investigated for lamellar polystyrene-*block*-polyisoprene-*block*-polydimethylsiloxane (SID) with symmetric composition and different block sequence ISD forming core-shell cylindrical with PDMS cores of relatively low molecular weight (10 k)<sup>29</sup>. The disordering process of the cylindrical structure takes place at a much lower temperature as compared to the lamellar structure, as shown in Figure 1-4. Besides, the symmetric polystyrene-*block*-polyisoprene-*block*-polystyrene (SIS) triblock copolymer is found to be approximate 20°C higher than that of the corresponding polystyrene-*block*-polyisoprene (SI) diblock copolymer<sup>30</sup>.

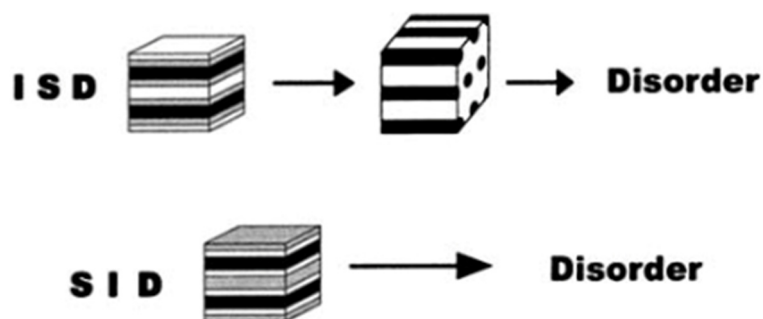


**Figure 1-4.** Schematic summary of thermodynamic phase behavior for PI-*b*-PS-*b*-PDMS (ISD) and PS-*b*-PI-*b*-PDMS (SID) copolymers. Decreasing molecular weight or heating ISD causes transition from three-domain lamellae to hexagonally packed two-domain cylindrical morphology, followed by disordering. In contrast, lamellar state directly transformed into disorder in SID case<sup>29</sup>.

### 1-3-3. Morphological Behavior of ABC Triblock Copolymer Melts

Many microdomain morphologies can be considered for ABC triblock copolymers by a simple combination of spherical, cylindrical, and lamellar shapes as shown in Figure 1-5. Various unique microdomain structures with highly regular periodicity such as knitting pattern<sup>25</sup> and ladder pattern<sup>31</sup> have also been theoretically predicted to exist in strong segregation limit by mean field theory<sup>32, 33</sup>.

For ABC triblock copolymers with short middle blocks and  $\chi$  parameters in the sequence of (A)  $\chi_{AC} < \chi_{AB} \approx \chi_{BC}$ , contact between A and C blocks is favorable, and the endblocks form the classical diblock domains with various shapes of B block domains decorating the A-C interfaces<sup>34-37</sup>; (B)  $\chi_{AC} > \chi_{AB} \approx \chi_{BC}$ , contact between A and C blocks is the least favorable, and alternating structures such as ABCCBA lamellae<sup>38</sup>, hexagonally alternating spheres<sup>39</sup>, and alternating gyroid<sup>21, 40</sup> would form; and (C)  $\chi_{AC} > \chi_{BC} > \chi_{AB}$ , spontaneous curvature would go toward on interface and core-shell structure is formed, such as core-shell cylinders<sup>39</sup> and core-shell gyroids<sup>23, 41</sup>.

Mogi et al.<sup>42</sup> and Gido et al.<sup>43</sup> reported the experiments on the effect of the sequence of blocks. They found that lamellar morphology is formed in polyisoprene-*block*-polystyrene-*block*-poly(2-vinylpyridine) (ISV) triblock with 1:1:1 composition, whereas in SIV with same composition the hexagonally-packed ordered cylinder phase is obtained as shown in Figure 1-6 (a) and 1-6 (b), respectively. The reason causing the different morphology of ISV and SIV triblocks lies in the different degrees of incompatibility between adjacent blocks in these two systems, as the

interaction parameter  $\chi_{SI} \approx \chi_{SV}$ . Further investigation about the influence of the block sequence on the morphological behavior of ABC triblock copolymers have revealed that the similar repulsive interactions between end and middle blocks lead to lamellar morphologies for even rather asymmetric composed ABC triblocks. In addition, when the interactions of the middle block towards the two endblocks is very dissimilar and the two endblocks are strongly incompatible with each other, there is a strong tendency to form core-shell morphologies. Core-shell analogues of the typical morphologies are known from diblock copolymers such as cylinders, double gyroid, and lamellae, can be obtained by varying the composition.

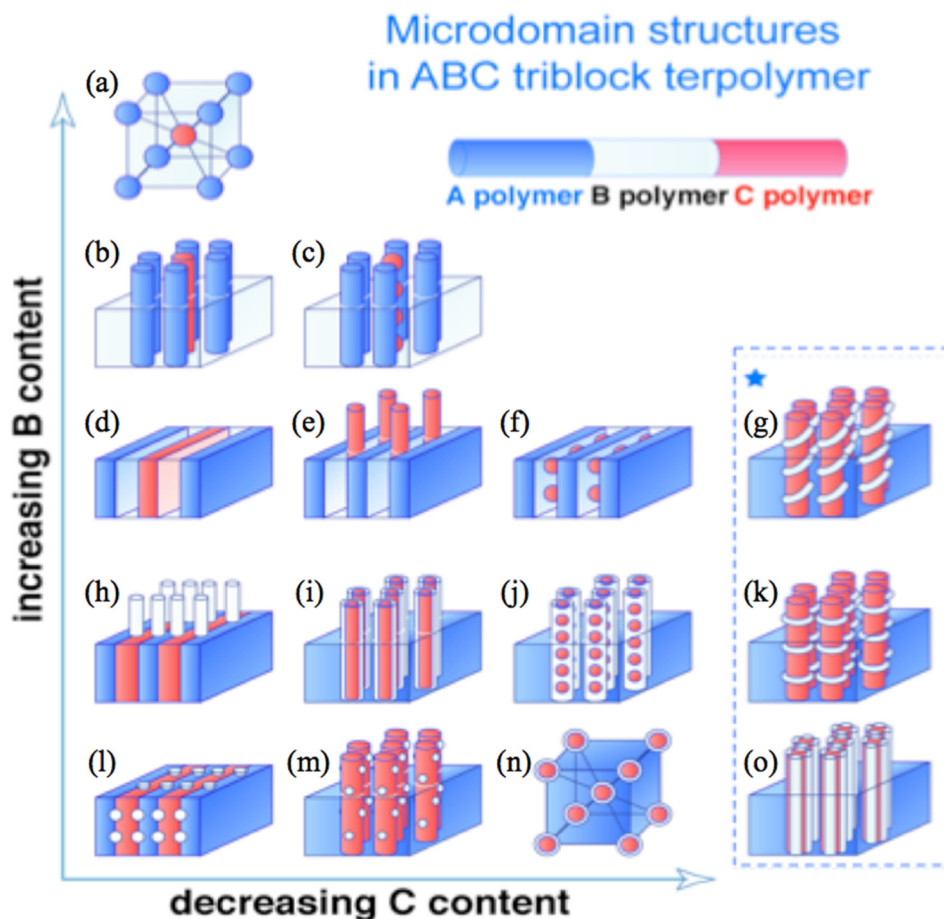


**Figure 1-5.** Schematic representation of possible microdomain morphologies considered of ABC triblock copolymers geometrically composed of spherical, cylindrical and lamellar microdomains. For the content marked with \* can be considered depending on the relative orientation of the different kinds of cylinders. (a) Spherical domains in the CsCl-type structure; (b) hexagonally-packed cylindrical domains; (d) lamellar phase; (e) lamella-cylinder-II; (f) lamella-sphere-II; (g) cylinder-ring phase; (h) lamella-cylinder phase; (i) coaxial cylinder phase; (j) cylinder-sphere; (l) lamella-sphere phase; (n) concentric spherical domain in the bcc structure.

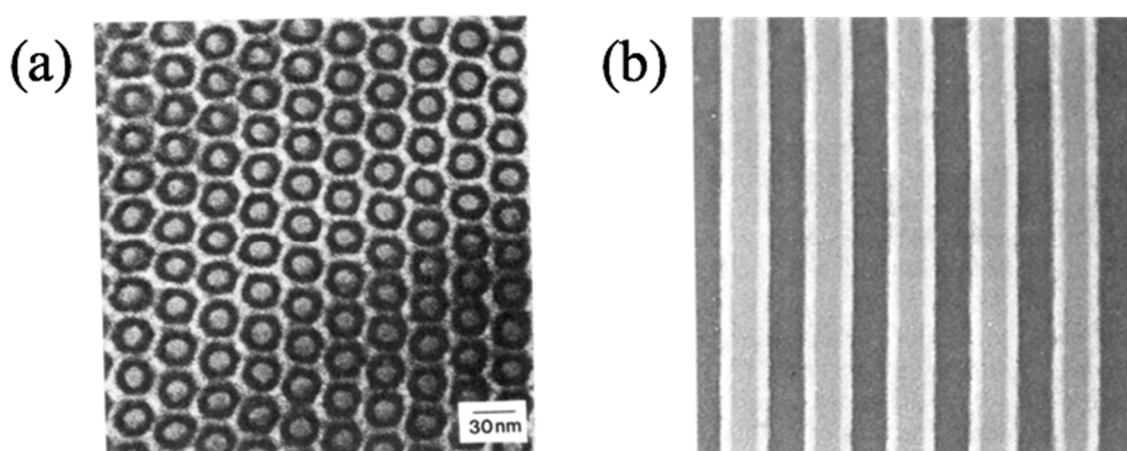


**Figure 1-6.** (a) Axial TEM projection of hexagonally-packed SIV triblock copolymers. The darkest regions correspond to the OsO<sub>4</sub>-stained PI domains, while the gray regions are CH<sub>3</sub>I-stained P2VP domains. (b) Electron micrograph of the three-phase lamellar structure of ISV triblock copolymer.

## 1-4. Ordered Network Morphology in Block Copolymer Melts

### 1-4-1. Introduction to Network Morphologies

Network morphologies have been found in diblock, triblock, starblock<sup>44</sup>, linear ABC triblock, and BCBA pentablock copolymers. Network morphology refers to a microstructure whose domain topology can be represented by a network lattice: connectivity of each node and the smallest number of such nodes that form a closed loop in the lattice. Schematic illustration for network morphologies in block copolymer is shown in Figure 1-7. Some network morphologies found in block copolymers have been cubic due to the isotropic nature of the forces driving self-assembly and the most familiar of these are the gyroid morphologies. They can be represented by a set of symmetric 3-fold junctions fitted with connectors<sup>45</sup>. An exception to this phenomenon was the identification of a noncubic network morphology in ABC triblock copolymers<sup>45</sup>, assigned to the *Fddd* space group with orthorhombic symmetry. Followed by the discovery of noncubic *Fddd*, a metastable orthorhombic *Pnna* space group was achieved by strong shear<sup>46</sup>. This class of network phases has similar structural elements with cubic networks (e.g., 3-fold junctions), but the junctions are not arranged in 3-fold symmetry. They contain three different unit cell lengths, thus they are flexible.

These network morphologies have multiply continuous structure and could be useful in many technological applications. Multiply continuous morphology allows each domain to directly contribute to the modulus<sup>47</sup>. Materials with three-dimensionally continuous structures have a great potential for application in nanotechnology such as

permeable membranes<sup>48</sup>, templates for the functional materials<sup>49, 50</sup>, and photonic crystals<sup>51, 52</sup>.

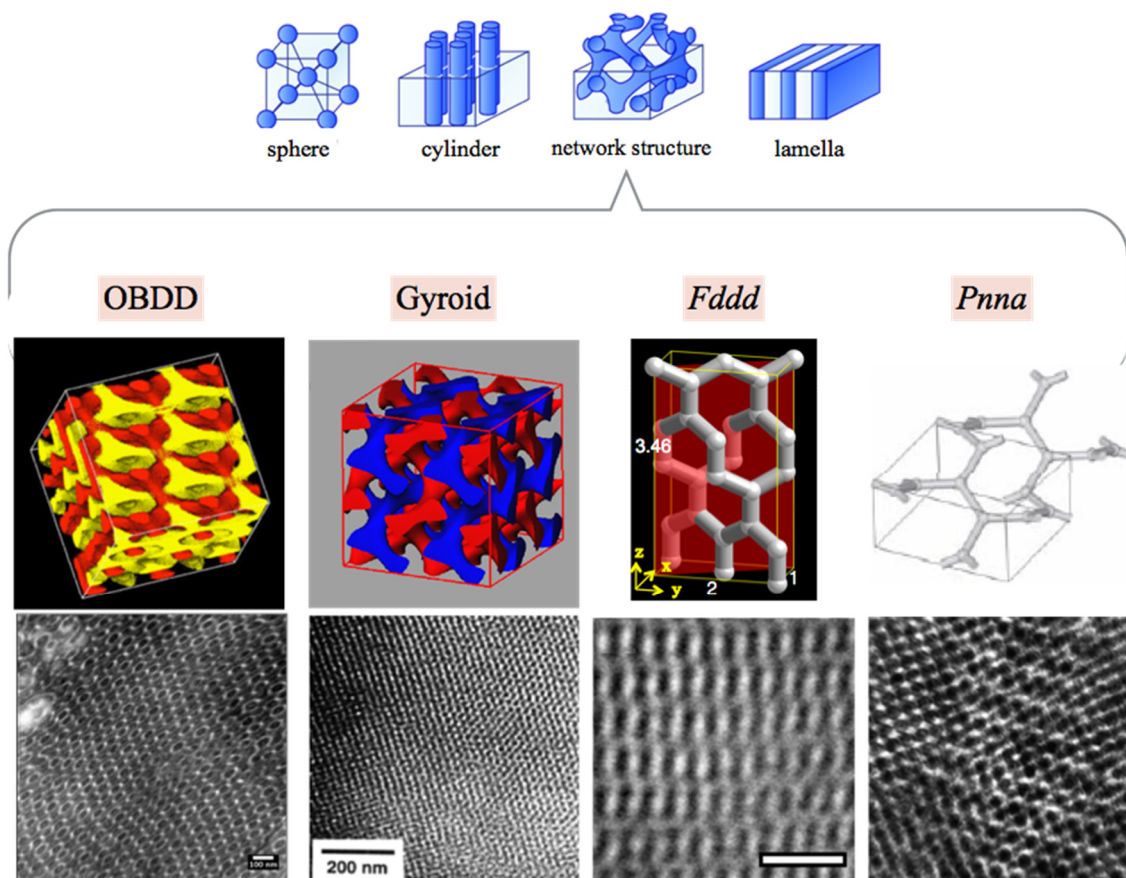


**Figure 1-7.** Schematic illustration for network morphologies. Upper panel: model representations of the network morphologies. Lower panel: Corresponding electron micrograph of network morphologies.

### 1-4-2. Ordered Bicontinuous Double-Diamond Morphology

Alward et al. characterized PS-*b*-PI starblock copolymer and first used “ordered bicontinuous” structure to describe block copolymer morphology<sup>44</sup>. OBDD was thereafter observed in diblock copolymers<sup>53, 54</sup>, diblock copolymer/ homopolymer blends<sup>55, 56</sup> and triblock copolymer/ homopolymer blends<sup>57</sup>. OBDD consists of tetrapod (4-fold) nodes connected with  $Pn3m$  symmetry. Transmission electron microscopy (TEM) images of OBDD and square arrangements are shown in Figure 1-8. As the first bicontinuous morphology found in block copolymers, a number of theoretical studies showed that OBDD was never predicted to be an equilibrium structure<sup>5, 58</sup> and the previously reported OBDD structures were identified as another bicontinuous structure, gyroid structure. Observation of stable OBDD phase in sPP-*b*-PS/ sPP and PS-*b*-PI/ PI blend system ensures the existence of the OBDD structure in the block copolymer/ homopolymer system<sup>56, 59</sup>.

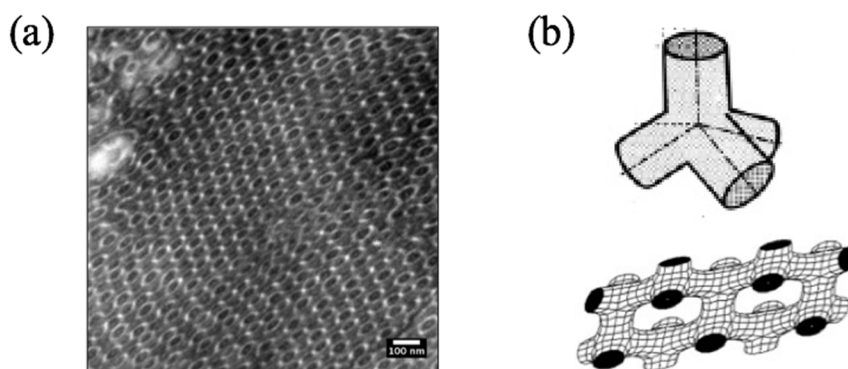


**Figure 1-8.** (a) Electron micrograph of PS-*b*-PI-*b*-PDMS triblock copolymer. (b) Tetrapod structural unit and six-membered ring arrangement of tetrapod in OBDD morphology.

### 1-4-3. Double Gyroid Network Morphology

An interpenetrating phase, which is located between cylinders and lamellae, called gyroid was reported in block copolymer by experimental groups<sup>14, 60, 61</sup>. Representative electron micrograph acquired from gyroid morphology is provided in Figure 1-9 (a). Gyroid is a bicontinuous cubic structure with  $Ia\bar{3}d$  symmetry, and the minority domain of gyroid forms left- and right-handed interweaving 3-fold constituent unit (Figure 1-7 (b)). Combination of SAXS characterization with relative  $q$  positions of  $\sqrt{3}$ ,  $\sqrt{4}$ ,  $\sqrt{10}$ ,  $\sqrt{11}$ ,  $\sqrt{16}$  and  $\sqrt{19}$  are identified. Gyroid is identified as a stable phase since it has the lowest amount of packing frustration<sup>62</sup>. The gyroid morphology is a widely accepted equilibrium structure in block copolymers following the considerable experimental<sup>63, 64</sup> and theoretical publications<sup>4, 65</sup>. Gyroid is anticipated to be used in a wide applicability such as 3D photonic crystals, nanoreactors, and so on<sup>66-68</sup>.

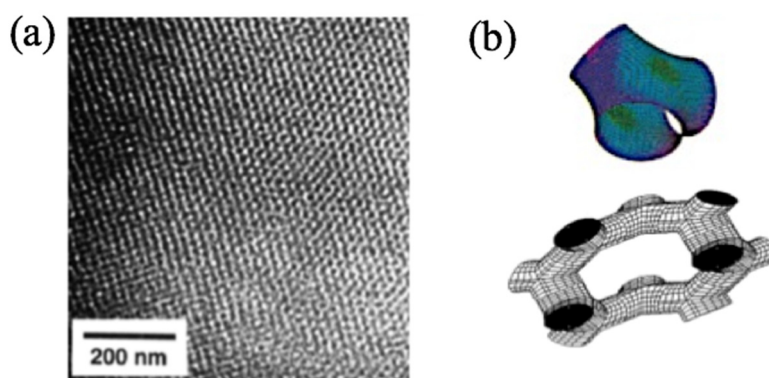


**Figure 1-9.** (a) Electron micrograph obtained from PS-*b*-PI diblock copolymer. (b) 3-fold symmetric unit of gyroid a six-membered ring planar structure.

#### 1-4-4. Orthorhombic *Fddd* Network Morphology

*Fddd* structure was firstly found in ISO triblock terpolymer<sup>69</sup>. Epps et al. confirmed this network morphology and characterized *Fddd* morphology as an equilibrium phase in ABC linear triblock copolymer<sup>70</sup>. Subsequently, *Fddd* structure was identified as an equilibrium phase in diblock copolymer melts within a narrow region<sup>6, 7, 71</sup>. Experimentally, it was reported that the *Fddd* structure was located between lamellar and gyroid phase in PS-*b*-PI diblock copolymer<sup>8, 9, 72</sup>. Figure 1-10 shows electron micrograph and the model illustration of the *Fddd* structure, *Fddd* structure has an orthorhombic unit cell with the lattice parameter ratio of  $a:b:c = 1:2:3.46$ . The image is similar to those obtained from gyroid morphology but do not possess any 3-fold or 4-fold symmetries. The bright oval shapes interconnected with the trivalent junctions are the characteristic of the *Fddd* network morphology. Due to its orthorhombic structure ( $a \neq b \neq c$ ), the *Fddd* structure exhibits optical anisotropy.

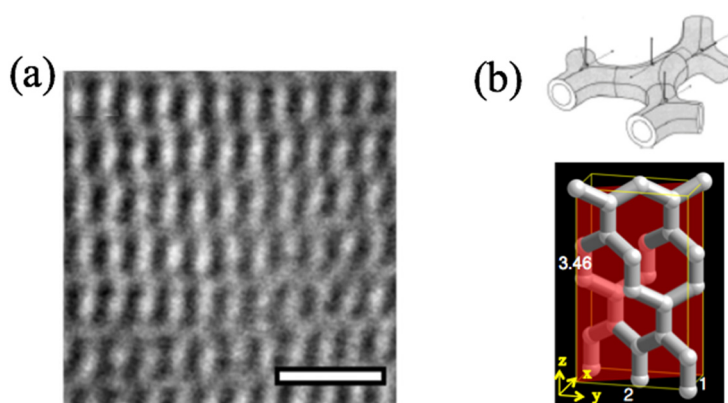


**Figure 1-10.** (a) Electron micrograph obtained from PS-*b*-PI diblock copolymer. (b) Representation of the corresponding *Fddd* network model with the TEM images in (a).

### 1-4-5. Orthorhombic *Pnna* Network Morphology

Discovery of the first orthorhombic *Fddd* network structure was followed by two investigations exhibiting another orthorhombic lattice morphology<sup>46, 73</sup>. This second network morphology possessing an orthorhombic lattice was named *Pnna* network as shown in Figure 1-11. By shearing the *Fddd*-forming poly(cyclohexylethylene-*b*-ethylethylene-*b*-ethylene) (CEEE) triblock copolymer, the SAXS data became different from that of *Fddd* and an orthorhombic space group with *Pnna* symmetry could fit the multiple orders of the reflections well. Similar to the *Fddd* morphology, *Pnna* has a 3-fold connector with mirror-plane symmetry and the networks are in an orthorhombic symmetry. Transformation between *Fddd* and *Pnna* can be achieved by changing the angle of 3-fold units. However, contrary to *Fddd* morphology, *Pnna* was reported as a metastable phase since *Fddd* is always obtained upon cooling below  $T_{ODT}$ .

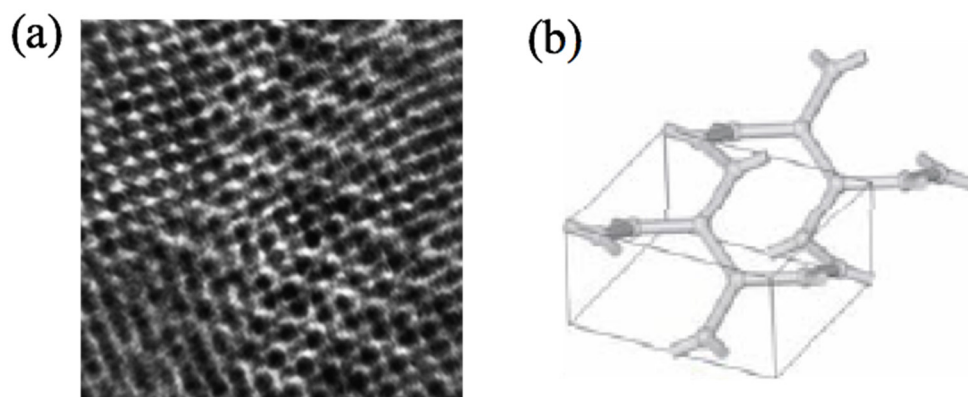


**Figure 1-11.** (a) Electron micrograph obtained from CEEE triblock copolymer. (b) Representations of *Pnna* network model.

## 1-5. Structural Analysis

### 1-5-1. Small-Angle X-ray Scattering

Small-angle X-ray scattering (SAXS) technique is extremely useful to investigate the structural properties in solid, liquid, gel or condensed matters, which have characteristic structure in the range of 10-100 nm. SAXS provides averaged information over the area irradiated by the X-ray beam (typically,  $0.1 \times 0.1 \text{ mm}^2$ ). In SAXS, we measure the scattered intensity of the sample irradiated by incident X-ray as a function of the scattering angle  $2\theta$ . The relevant parameter to analyze the interaction is the momentum transfer or scattering vector  $\mathbf{q}$ , defined by

$$|\mathbf{q}| = \frac{4\pi \sin\theta}{\lambda} \quad (1.1)$$

Domain size of the periodic structures in the materials can be obtained by Bragg's law from the intensity maxima of the scattering patterns,

$$n\lambda = 2d\sin\theta \quad (1.2)$$

where  $d$  is the repeat distance in the periodic structure or the d-spacing between the crystallographic planes,  $2\theta$  is the scattering angle. Then, Bragg's law can be combined with the magnitude of scattering vector  $q$ :

$$|\mathbf{q}| = \frac{2n\pi}{d} \quad (1.3)$$

SAXS profiles are representative of an entire sample, thus SAXS provides an alternative interpretation and can be viewed as a complement method. In block copolymer systems, the allowed reflections for commonly known morphologies are

listed in Table 1-1.

**Table 1.1.** Allowed peak reflections for morphologies of block copolymers.

<b>Morphology</b>	<b>Abbreviation</b>	<b>Allowed Reflections</b>
Lamellae	LAM	1: 2: 3: 4: 5: 6...
<i>Fddd</i>	<i>Fddd</i>	1: 1.22: 1.58: 1.73: 1.8: 1.93...
<i>Pnna</i>	<i>Pnna</i>	1: 1.41: 2: 2.24: 2.82...
Gyroid	<i>Ia<math>\bar{3}d</math></i>	1: 1.15: 1.53: 1.63: 1.83: 1.91...
OBDD	OBDD	1: 1.22: 1.41: 1.73: 2: 2.12...
Hexagonally Packed Cylinders	HEX	1: $\sqrt{3}$ : $\sqrt{4}$ : $\sqrt{7}$ : $\sqrt{9}$ : $\sqrt{12}$ ...
Spheres (Body-Centered Cubic Lattice)	BCC	1: $\sqrt{2}$ : $\sqrt{3}$ : $\sqrt{4}$ : $\sqrt{5}$ : $\sqrt{6}$ ...

### 1-5-2. Electron Tomography

Combing the computed tomography (CT) technique with TEM<sup>74</sup>, electron tomography has become a useful tool to visualize the complex 3D structure of materials, grain boundaries in various systems<sup>75-77</sup>.

The principle of electron tomography outlined by Radon<sup>78</sup> is shown in Figure 1-12. The structure of the object,  $f(x, y)$ , can be reconstructed from the projection at angle  $\theta$ ,  $p(r, \theta)$  by the inverse Radon transform. Basically, the reconstruction of the object from the projection can be done by the “projection slice theorem”, which states that one-dimensional Fourier transformation of the projection of one section of an object at angle  $\theta$  coincides with the central line have the same angle in two-dimensional Fourier space. Full range of Fourier transform of the density distribution in the object can thus be obtained from Fourier transform of a series projections.

The limitation of the angular range of image collection during TEM observation makes it lack of the information in the high-frequency area. To solve this problem, “weighted back projection” (WBP) or “filtered back projection” (FBP) are introduced into electron tomography technique. In these two methods, lines are gathered in the center of Fourier space and corrected by a weighting filter, which is a radial linear function, zero at the center and maximum at the edge. By using inverse Fourier transform of a series of projections for an object multiplied by the filter function, 3D-reconstructed image can be obtained in real space.

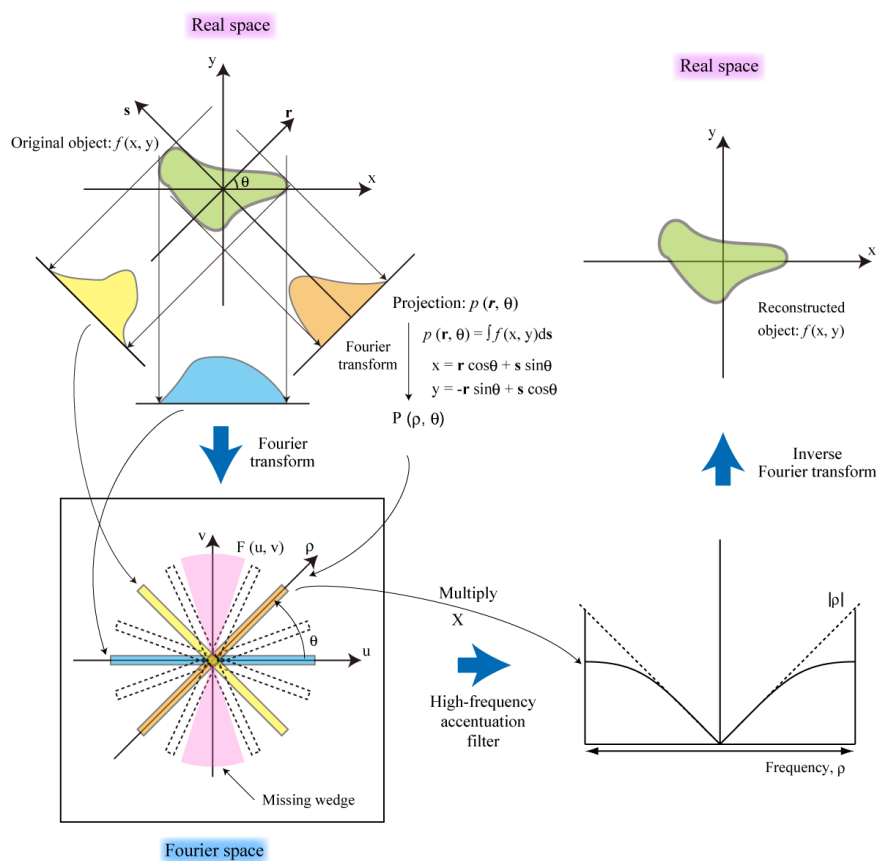


**Figure 1-12.** Illustration of the principle and process of electron tomography.

However, the resolution of the 3D-reconstructed image is reduced in the direction parallel to the electron beam due to the limitation of the achievable tilting angle ( $\theta = \pm 60^\circ \sim 70^\circ$ ) of the objective lens in electron tomography. Several efforts such as dual-axis tomography<sup>79</sup> and complete rotation with a rod-shaped sample<sup>80-81</sup> have been developed in correspondence to this problem.

## 1-6. Contents of this thesis

In this thesis, I aimed to control the network morphology on the basis of the following techniques and to clarify the mechanism of the self-assembly with the following techniques. (1) Composition control of block copolymer. By directly synthesizing the specific composition of diblock copolymer, the desired network morphology can be obtained in the corresponding composition window. (2) Addition of homopolymer. By blending the homopolymer into the corresponding diblock copolymer, network structure that is not observed in the neat diblock copolymer can be obtained. (3) Architectural design of block-graft copolymer. By varying the architecture of diblock copolymer, network structure can also be obtained (4). Two-step microphase separation of triblock copolymer. Network structure could be obtained through step ordering process. The first-step of two-step microphase separation is similar with that in diblock copolymers, and the knowledge about the morphological control have been studied extensively in diblock copolymers. (5) Solvent cast method with mixed-solvent. The effective composition of the individual block and the resulting morphology in the block copolymer can be varied with the aid of mix-solvent technique.

This thesis contains two main parts. Part 1 consists of chapter 2 and 3 concerning about discovery of orthorhombic  $Fddd$  network morphology in diblock copolymer and diblock copolymer/ homopolymer blends. Part 2 consists of chapter 4, 5, and 6 for the detail observation of OBDD via electron microscope, investigation of OBDD-forming process and tunability of ordered morphologies with the aids of mixed-solvent technique.

In Chapter 2, the *Fddd* phase in polystyrene (PS) rich region of the phase diagram for polystyrene-*block*-polyisoprene (SI) diblock copolymers is investigated. Five SI diblock copolymer samples with volume fraction rich in PS were prepared and the *Fddd* phase was found as an equilibrium phase in the range of  $0.37 \leq f_{PI} \leq 0.373$  and  $19.5 < \chi N < 21.1$ . Compared to the *Fddd* phase in PI-rich region, the *Fddd* phase boundary in PS-rich region is much narrower than that in PI-rich region. The conformational asymmetry between PS and PI chains would be responsible for the asymmetry of *Fddd* regime between PS-rich and PI-rich region.

In chapter 3, the *Fddd* structure in polystyrene-*block*-polyisoprene (SI) diblock copolymer/ polystyrene (hPS) homopolymer was observed. By SAXS and TEM, the *Fddd* phase was found as an equilibrium phase in the range of  $0.632 \leq f_{PI} \leq 0.641$  and  $27.5 < \chi N < 30.2$ . The *Fddd* phase boundary in the SI/ hPS is similar to that in the neat SI block copolymer since the hPS with the low molecular weight does not change the critical point  $(\chi N)_c$  for the microphase separation of the blends.

In chapter 4, OBDD network morphology was found in polystyrene-*block*-(poly-4-vinylphenyldimethylvinylsilane-*graft*-polyisoprene), PS-*b*-(PVPDVS-*g*-PI), block-*graft* copolymer. According to the TEM analysis, it is identified that the constituting unit of the structure is a tetrapod comprise of four rodlike segments of major PS phase. These tetrapod units join together as a planar six-membered ring and form an ordered three-dimensional OBDD network and the minor PI fills up the matrix phase. The architecture of PS-*b*-(PVPDVS-*g*-PI) block-*graft* copolymer is the dominant factor for the inverse formation of the OBDD network structure.

In chapter 5, the ordered bicontinuous double-diamond morphology (OBDD) was found in polystyrene-*block*-polyisoprene-*block*-polydimethylsiloxane (code: SID1) triblock copolymer film cast from toluene solution. Via SAXS, self-assembly process during solvent cast was studied. In the early stage of the cast process, PDMS cylinders packed hexagonally in PS/PI matrix where PS and PI were in homogeneous state. Then order-order transition from cylinder to OBDD induced by the microphase separation between PS and PI occurred as toluene solvent evaporated. We expected that the two-step phase separation could induce the metastable structure such as OBDD network structure.

In chapter 6, various ordered structures such as spheres, hexagonally-packed cylinders, lamellae, OBDD network structure were obtained in the polystyrene-*block*-polyisoprene-*block*-polydimethylsiloxane (code: SID2) triblock copolymer by using mixed-solvent with different weight ratio of toluene and n-decane. More importantly, structures that were found in the solution can be preserved in bulk state. The effects of varying the ratio between two solvents and the concentration of the mixed-solvent used during the casting process on the microphase separation of SID triblock copolymer are demonstrated.

## Reference

1. Szwarc, M. *Nature* **1956**, 178, 1168-1169.
2. Miyamoto, M.; Sawamoto, M.; Higashimura, T. *Macromolecules* **1984**, 17, 265-268.
3. Otsu, T.; Yoshida, M.; Kuriyama, A. *Polym. Bull.* **1982**, 7, 44-50.
4. Matsen, M. W.; Schick, M. *Phys. Rev. Lett.* **1994**, 72, 16, 2660-2663.
5. Matsen, M. W.; Bates, F. S. *Macromolecules* **1996**, 29, 4, 1091-1098.
6. Tyler, C. A.; Morse, D. C. *Phys. Rev. Lett.* **2005**, 94, , 208302/1-208302/4.
7. Ranjan, A.; Morse, D. C. *Physical Review E* **2006**, 74, 011803.
8. Takenaka, M.; Wakada, T.; Akasaka, S.; Nishitsuji, S.; Saijo, K.; Shimizu, H.; Kim, M. I.; Hasegawa, H. *Macromolecules* **2007**, 40, 4399-4402.
9. Kim, M. I.; Wakada, T.; Akasaka, S.; Nishitsuji, S.; Saijo, K.; Hasegawa, H.; Ito, K.; Takenaka, M. *Macromolecules* **2008**, 41, 7667-7670.
10. Wang, Y. C.; Matsuda, K.; Kim, M. I.; Miyoshi, A.; Akasaka, S.; Nishitsuji, S.; Saijo, K.; Hasegawa, H.; Ito, K.; Hikima, T.; Takenaka, M. *Macromolecules* **2015**, 48, 2211-2216.
11. Hamley, I. W. *The Physics of Block Copolymers*. Oxford University Press: New York, **1998**.
12. Bates, F. S.; Fredrickson, G. H. *Physics Today* **1999**, 52, 32.
13. V. E. Podnepska and I. W. Hamley *Pis'mav. ZhETF* **1996**, 64, 564-569.

14. Khandpur, A. K.; Forster, S.; Bates, F. S.; Hamley, I. W.; Ryan, A. J.; Bras, W.; Almdal, K.; Mortensen, K. *Macromolecules* **1995**, 28, 8796-8806.
15. Matsen, M. W. *Eur. Phys. J. E* **2009**, 30, 361-369.
16. Hadjichristidis, N.; Iatrou, H.; Behal, S. K.; Chludzinski, J. J.; Disko, M. M.; Garner, R. T.; Liang, K. S.; Lohse, D. J.; Milner, S. T. *Macromolecules* **1993**, 26, 5812-5815.
17. Bellas, V.; Iatrou, H.; Hadjichristidis, N. *Macromolecules* **2000**, 33, 6993-6997.
18. Stadler, R.; Auschra, C.; Bechmann, J.; Krappe, U.; Voigtmartin, I.; Leibler, L. *Macromolecules* **1995**, 28, 3080-3097.
19. Wei, Z.; Wang, Z. G. *Macromolecules* **1995**, 28, 7215-7223.
20. Matsen, M. W. *J. Chem. Phys.* **1998**, 108, 785-796.
21. Matsushita, Y.; Suzuki, J.; Seki, M. *Physics B* **1998**, 248, 238-242.
22. Breiner, U.; Krappe, U.; Thomas, E. L.; Stadler, R. *Macromolecules* **1998**, 31, 135-141.
23. Shefelbine, T. A.; Vigild, M. E.; Matsen, M. W.; Hadjuk, D. A.; Hillmyer, M. A.; Cussler, E. L.; Bates, F. S. *J. Am. Chem. Soc.* **1999**, 121, 8457-8465.
24. Huckstadt, H.; Goldacker, T.; Gopfert, A.; Abetz, V. *Macromolecules* **2000**, 33, 3757-3761.
25. Takahashi, K.; Hasegawa, H.; Hashimoto, T.; Bellas, V.; Iatrou, H.; Hadjichristidis, N. *Macromolecules* **2002**, 35, 4859-4861.
26. Takano, A.; Soga, K.; Asari, T.; Suzuki, J.; Arai, S.; Saka, H.; Matsushita, Y.

- Macromolecules* **2003**, 36, 8216-8218.
27. Kaneko, T.; Suda, K.; Satoh, K.; Kamigaito, M.; Kato, T.; Ono, T.; Nakamura, E.; Nishi, T.; Jinnai, H. *Macromolecular Symposia* **2006**, 242, 80-86.
28. Erukhimovich, E.; Abetz, V.; Stadler, R. *Macromolecules* **1997**, 30, 7435-7443.
29. Hardy, C.M.; Bates, F.S.; Kim, M. H.; Wignall, G.D.; *Macromolecules* **2002**, 35, 3189-3197.
30. Choi, S.; Vaidya, N. Y.; Han, C.D.; Sota, N.; Hashimoto, T. *Macromolecules* **2003**, 36, 7707-7720.
31. Kaneko, T.; Suda, K.; Satoh, K.; Kamigaito, M.; Kato, T.; Ono, T.; Nakamura, E.; Nishi, T.; Jinnai, H. *Macromolecular Symposia* **2006**, 242, 80-86.
32. Phan, S.; Fredrickson, G.H. *Macromolecules* **1998**, 31, 59-63.
33. Dotera, T. *Physical Phys. Rev. Lett.* **2002**, 89, 205502.
34. Auschra, C.; Stadler, R. *Macromolecules* **1993**, 26, 2171-2174.
35. Krappe, U.; Stadler, R.; Voigt-Martin, I. *Macromolecules* **1995**, 28, 4558-4561.
36. Breiner, U.; Krappe, U.; Abetz, V.; Stadler, R. *Macromol. Chem. Phys.* **1997**, 198, 1051-1083.
37. Breiner, U.; Krappe, U.; Jakob, T.; Abetz, V.; Stadler, R. *Polym. Bull.* **1998**, 40, 219-226.
38. Brinkmann, S.; Stadler, R.; Thomas, E. *Macromolecules* **1998**, 31, 6556-6558.
39. Mogi, Y.; Nomura, M.; Kotsuji, H.; Ohnishi, K.; Matsushita, Y.; Noda, I.

- Macromolecules* **1994**, 27, 6755-6760.
40. Suzuki, J.; Seki, M.; Matsushita, Y. *J. Chem. Phys.* **2000**, 112, 4862-4868.
41. Abetz, V.; Goldacker, T. *Macromol. Rapid Commun.* **2000**, 21, 16-34.
42. Mogi, Y.; Mori, K.; Kotsuji, H.; Matsushita, Y.; Noda, I.; Han, C. C. *Macromolecules* **1993**, 26, 5169-5173.
43. Gido, S. P.; Sschwark, D. W.; Thomas, E. L.; Goncalves, M. D. *Macromolecules* **1993**, 26, 2636-2640.
44. Alward, D. B.; Kinning, D. J.; Thomas, E. L.; Fetters, L. J. *Macromolecules* **1986**, 19, 215-224.
45. Epps III, T. H.; Cochran, E. W.; Hardy, C. M.; Bailey, T. S.; Waletzko R. S.; Bates, F. S. *Macromolecules* **2004**, 37, 8325-8341.
46. Cochran, E. W.; Bates, F. S. *Phys. Rev. Lett.* **2004**, 93, 087802/1-087802/4.
47. Potschke, P.; Paul, D. R. *J. Macromol. Sci., Polym. Rev.* **2003**, C43, 87-141.
48. Milhaupt, J. M.; Lodge, T. P. *J. Polym. Sci. Part B Polym. Phys.* **2001**, 39, 843-859.
49. Mao, H. M.; Hillmyer, M. A. *Soft Matter* **2006**, 2, 57-59.
50. Urade, V. N.; Wei, T. C.; Tate, M. P.; Kowalski, J. D.; Hillhouse, H. W. *Chemistry of Material* **2007**, 19, 768-777.
51. Martin-Moreno, L.; Garcia-Vidal, F. J.; Somoza, A. M. *Phys. Rev. Lett.* **1999**, 83, 73-75.
52. Maldovan, M.; Urbas, A. M.; yufa, N.; Carter, W. C. Thomas, E. L. *Phys. Rev. B* **2001**, 39, 843-859.

53. Thomas, E. L.; Alward, D. B.; Kinning, D. J.; Martin, D. C.; Handlin, D. L.; Fetters, L. J. *Macromolecules* **1986**, 19, 2197-2202.
54. Hasegawa, H.; Tanaka, H.; Yamasaki, K.; Hashimoto, T. *Macromolecules* **1987**, 20, 1651-1662.
55. Winey, K. I.; Thomas, E. L.; Fetters, L. J. *Macromolecules* **1992**, 25, 422-428.
56. Takagi, H.; Yamamoto, K.; Okamoto, S. *Europhys. Lett.* **2015**, 110, 48003/p1-p6.
57. Xie, R.; Yang, B.; Jiang, Bingzheng. *Macromolecules* **1993**, 26, 7097-7099.
58. Masten, M. W.; Scick, M. *Macromolecules* **1994**, 27, 6761-6767.
59. Chu, C. Y.; Lin, W. F.; Tsai, J. C.; Lai, C. S.; Lo, S. C.; Chen, H. L.; Hashimoto, T.; *Macromolecules* **2012**, 45, 2471-2477.
60. Hajduk, D. A.; Harper, P. E.; Gruner, S. M.; Honeker, C. C.; Kim, G.; Thomas, E. L.; Fetters, L. J. *Macromolecules* **1994**, 27, 4063-4075.
61. Schoen, A. H. NASA TN D-5541, **1970**.
62. Matsen, M. W.; Bates, F. S. *Macromolecules* **1996**, 29, 7641-7646.
63. Schulz, M. F.; Bates, F. S.; Almdal, K.; Mortensen, K. *Phys. Rev. Lett.* **1994**, 73, 86-89.
64. Hajduk, D. A.; Harper, P. E.; Gruner, S. M.; Honeker, C. C.; Thomas, E. L.; Fetters, L. J. *Macromolecules* **1995**, 28, 2570-2573.
65. Matsen, M.W. Bates, F.S. *J. Chem. Phys.* **1997**, 106, 2436-2448.
66. Alexander, C. E.; Augustine, M. U.; DeRege, P.; Chen, C. X.; Swager, T. M.; Hadjichristidis, N.; Xenidou, M.; Fetters, L. J.; Joannopoulos, J. D.; Fink, Y.;

- Thomas, E. L. *Adv. Mater.* **2001**, *13*, 421-425.
67. Hashimoto, T.; Tsutsumi, K.; Funaki, Y. *Langmuir* **1997**, *13*, 6869-6872.
68. Chan, V. Z.-H.; Hoffman, J.; Lee, V. Y.; Iatrou, H.; Avgeropoulos, A.; Hadjichristidis, N.; Miller, R. D. *Science* **1999**, *286*, 1716-1719.
69. Bailey, T. S.; Hardy, C. M.; Epps, T. H.; Bates, F. S. *Macromolecules* **2002**, *35*, 7007-7017.
70. Epps, T. H.; Cochran, E. W.; Hardy, C. M.; Bailey, T. S.; Waletzko, R. S.; Bates, F. S. *Macromolecules* **2004**, *37*, (19), 7085-7088.
71. Yamada, K.; Nonomura, M.; Ohta, T. *J. Phys.: Condens. Matter* **2006**, *18*, L421-L427.
72. Kim, M. I.; Wakada, T.; Akasaka, S.; Nishitsuji, S.; Saijo, K.; Hasegawa, H.; Ito, K.; Takenaka, M. *Macromolecules* **2009**, *42*, 5266-5271.
73. Bluemle, M. J.; Fleury, G.; Lodge, T. P.; Bates, F. S. *Soft Matter* **2009**, *5*, 1587-1590.
74. Frank, J., *Electron Tomography*. 2nd ed.; Springer: New York, 2005.
75. Jinnai, H.; Kaneko, T.; Nishioka, H.; Hasegawa, H.; Nishi, T. *Chemical Record* **2006**, *6*, (5), 267-274.
76. Nishioka, H.; Niihara, K. I.; Kaneko, T.; Yamanaka, J.; Inoue, T.; Nishi, T.; Jinnai, H. *Composite Interfaces* **2006**, *13*, (7), 589-603.
77. Jinnai, H.; Shinbori, Y.; Kitaoka, T.; Akutagawa, K.; Mashita, N.; Nishi, T. *Macromolecules* **2007**, *40*, (18), 6758-6764.
78. Radon, J. *Math. -Phys. Klasse* **1917**, *69*, 262-277.

79. Sugimori, H.; Nishi, T.; Jinnai, H. *Macromolecules* **2005**, 38, (24), 10226-10233.
80. Kaneko, T.; Nishioka, H.; Nishi, T.; Jinnai, H. *Journal of Electron Microscopy* **2005**, 54, (5), 437-444.
81. Kato, M.; Kawase, N.; Kaneko, T.; Toh, S.; Matsumura, S.; Jinnai, H. *Ultramicroscopy* **2008**, 108, (3), 221-229.

## *Chapter 2*

# **Orthorhombic *Fddd* Microdomain Structure in Diblock Copolymer**

### **2-1. Introduction**

Matsen and Schick predicted the following four morphologies exist as equilibrium structures: lamellae (L), gyroid (G), hexagonally packed cylinder (C), and sphere in the body-centered lattice (S) by using self-consistent-field theory (SCFT)<sup>1</sup>, and the result of SCFT agrees with the phase diagram obtained experimentally for polystyrene-*block*-polyisoprene (SI) diblock copolymer. Experimentally, the phase diagram for SI diblock copolymer near order-disorder transition has been constructed by Khandpur<sup>2</sup>. They determined the phase boundaries of L, G, C, and S, and they found qualitative agreement between experimental and theoretical phase diagram<sup>2, 3</sup>.

In addition to the morphologies mentioned above, it has been found that *Fddd*

structure exists as an equilibrium phase in diblock copolymer melts. Tyler and Morse reexamined the phase diagram of diblock copolymers and predicted that *Fddd* phase is also stable in diblock copolymer melts within a narrow region<sup>4</sup>. Yamada et al.<sup>5</sup>, Ranjan and Morse<sup>6</sup> also found *Fddd* structure is stable in diblock copolymers theoretically. Experimentally the previous study explored the *Fddd* structure exists between L and G phases in SI diblock copolymer<sup>7</sup>. They checked the stability of *Fddd* structure after long time annealing and the thermoreversibility, and confirmed that the *Fddd* structure exists as an equilibrium structure in SI diblock copolymer<sup>8</sup>. They also found that the stable region of *Fddd* phase exists at  $0.629 \leq f_{PI} \leq 0.649$  and  $25.6 < \chi N < 29.8$ <sup>9</sup>. Jung et al. also found *Fddd* phase in SI ( $f_{PI} = 0.645$ ) thin film<sup>10</sup>. The existence of *Fddd* phase at the polyisoprene (PI) rich region or  $f_{PI} > 0.5$  was proved. It is anticipated that the *Fddd* phase should exist on the other side of phase diagram, which is polystyrene (PS)-rich region or  $f_{PI} < 0.5$ . Ahn et al. have already found that *Fddd* structure coexists with G in PS-rich region of SI diblock copolymer melts, the detail of the *Fddd* phase in PS-rich region, however, has not examined yet.

In this chapter, we synthesized five SI diblock copolymers with various compositions in PS-rich region and investigated their phase behaviors by small-angle X-ray scattering (SAXS) and transmission electron microscope (TEM). Then the stable region of the *Fddd* structure and the phase boundary were determined in PS-rich region of SI diblock copolymers.

## 2-2. Experimental Section

Five SI diblock copolymer samples were synthesized via living anionic polymerization at 50°C in benzene under an argon environment using *sec*-BuLi as an initiator. Number-average molecular weight ( $M_n$ ) and polydispersity index (PDI) of SI diblock copolymers were determined by size exclusion chromatography (SEC) using polystyrene standards. For SEC measurement, THF was used as the eluent at 40°C and the chromatograms were recorded with a refractive index detector. Volume fraction of polyisoprene ( $f_{PI}$ ) was determined by using  $^1H$  nuclear magnetic resonance (NMR) spectroscopy. We also identified that polyisoprene has a high degree of 1,4-addition (more than 95%) and a small degree of 3,4-addition (less than 5%) by NMR. The characterizations of the samples are listed in Table 2-1. Prior to each experiment, we made 5wt% polymer solution in toluene with 0.2wt% 2,6-di-*tert*-butyl-4-methylphenol as an anti-oxidant agent and then cast them at 30°C for 1 week. The cast films were further dried at room temperature in vacuum for 1 day. Thickness of the as-cast films is about 0.1mm. We applied post-annealing in SAXS sample holder where the sample thickness sandwiched by Kapton films is 2.5mm.

**Table 2-1.** Molecular Characteristics of SI Diblock Copolymers.

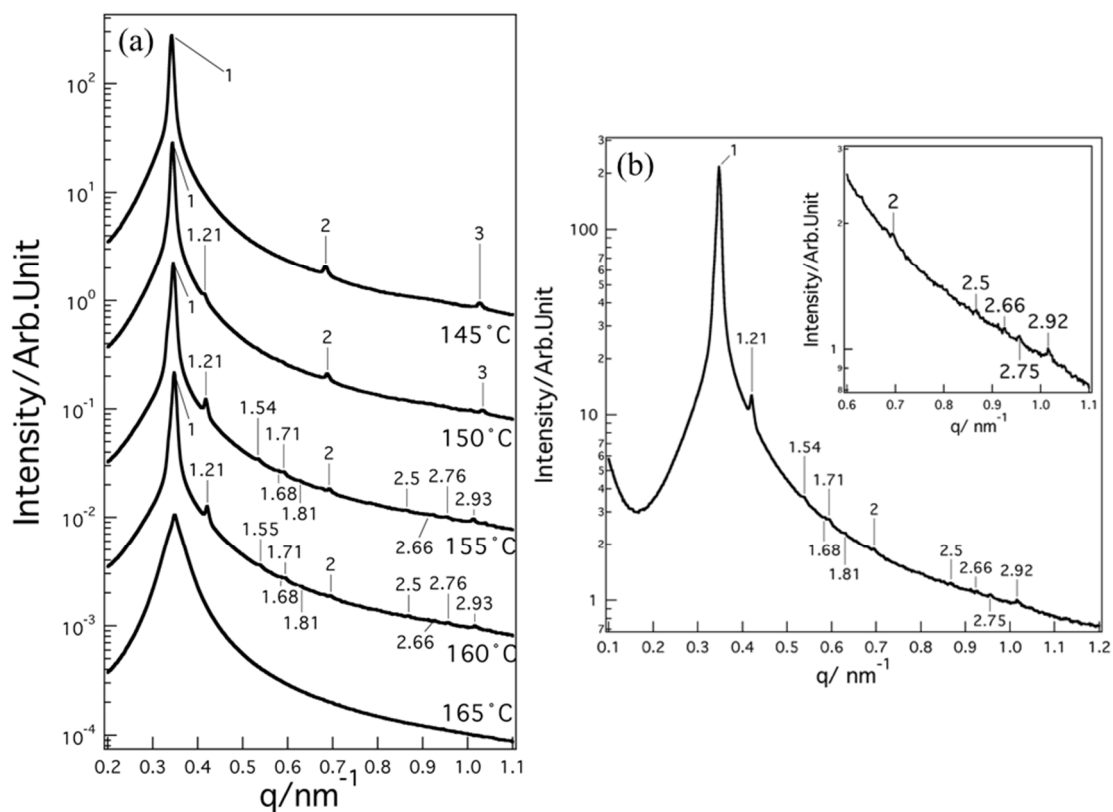
Code	$M_n (\times 10^4) (\text{g} \cdot \text{mol}^{-1})$	$f_{PI}$	$M_w/M_n$
I1	3.06	0.367	1.01
I2	3.71	0.370	1.03
I3	2.16	0.373	1.01
I4	1.94	0.379	1.01
I5	2.54	0.385	1.03

## 2-3. Results and Discussion

Figure 2-1 (a) shows the temperature dependence of SAXS profiles of I3 ( $f_{PI} = 0.373$ ). The scattered intensity  $I(q)$  is plotted as a function of wave number  $q$  ( $q = (4\pi/\lambda)\sin(\theta/2)$ ;  $\theta$  is scattering angle and  $\lambda$  is wavelength). Below 165°C, several distinct peaks appear, indicating that I3 is in ordered state. At 145 and 150°C, the peaks at  $q/q_m = 1, 2,$  and  $3$  are showed in the SAXS profiles with  $q_m = 0.342$  and  $0.344 \text{ nm}^{-1}$ , respectively. These integer multiples of  $q_m$  indicates that the lamellar structure was formed in I3 at 145 and 150°C. On the other hand, at 155 and 160°C, the ratios of  $q/q_m$  become different from those of the lamellar structure. SAXS peaks are located at  $q/q_m = 1, 1.21, 1.54, 1.68, 1.71, 1.81, 2.00, 2.50, 2.65, 2.76,$  and  $2.93$  with  $q_m = 0.344 \text{ nm}^{-1}$ . Enlarged SAXS profile at 155°C is shown in Figure 2-1 (b). This series agrees with the peak ratio of the *Fddd* structure in SI diblock copolymer<sup>7</sup>. These peaks can be indexed as 111, 004 ( $q/q_m = 1$ ), 113 (1.21), 115 and 131 (1.54), 040 (1.68), 133 (1.71), 202 (1.81), 222 (2.00), 242 (2.47), 311 (2.67), 313 (2.75), 315 (2.92). We estimated ( $a:b:c$ ) = (1:2.08:3.62) with  $a = 20.7 \text{ nm}$  by using

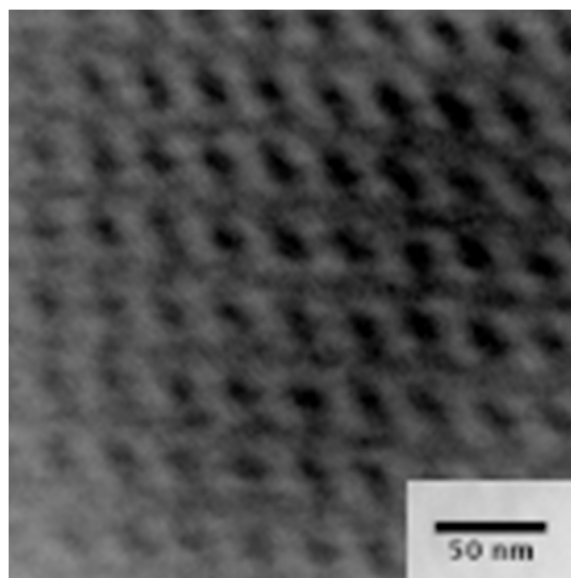
$$q_{hkl} = 2\pi[h^2/a^2 + k^2/b^2 + l^2/c^2]^{1/2}, \quad (1)$$

where  $a, b,$  and  $c$  are unit cell parameters and  $h, k,$  and  $l$  are Miller indices for  $a, b,$  and  $c,$  respectively. At 165°C a single broad peak is observed suggesting that I3 is in disordered state at 165°C.



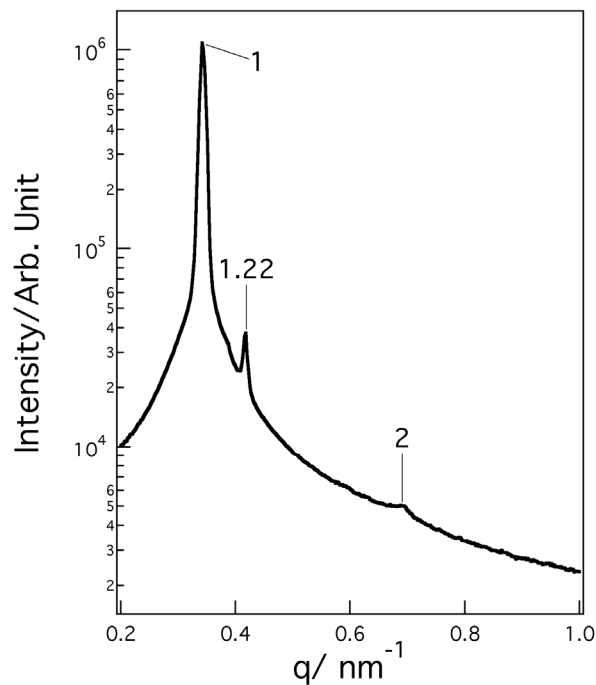
**Figure 2-1.** (a) Temperature dependence of SAXS profiles for I3 ( $f_{PI} = 0.373$ ). The profiles are shifted vertically to avoid overlapping. (b) SAXS profile at 155°C, inset is enlarged part of high  $q$ -regime.

Figure 2-2 shows the TEM image of I3 at 160°C. The black ovals are connected with trivalent junctions in the TEM image, which are representative patterns of *Fddd* structure, agreeing with the results of SAXS profile. The results of SAXS and TEM for I3 indicate that I3 exhibits L-*Fddd*-Disorder transition. This transition does not contain *Fddd*-G transition, which is different from the phase behavior of *Fddd* in PI-rich region<sup>8</sup>.



**Figure 2-2.** TEM image of I3 at 160°C. The pattern of the staggered rows of bright areas suggests a network structure interconnected with trivalent junctions.

In order to check whether the  $Fddd$  phase exists as an equilibrium phase at  $f_{P1} < 0.5$ , we examined the stability of the  $Fddd$  structure. We checked the stability of  $Fddd$  structure after long time annealing, and the thermoreversibility between L and  $Fddd$  structure. Figure 2-3 shows the SAXS profile after long time annealing at 155°C. Even after 31 hours, we still found  $q/q_m = 1.22$ , characteristic peak of  $Fddd$ , indicating that  $Fddd$  survives after long time annealing.



**Figure 2-3.** SAXS profile of I3 annealing at 155°C after 31 hours.

Figure 2-4 shows the result on the check of thermoreversibility between L and  $Fddd$ . First we annealed I3 at 125°C, where L is stable, for 24 hours. Figure 2-4 (a) is SAXS profile after annealing at 125°C and we found L is stable at 125°C. Subsequently,

I3 was annealed at 155°C for 20 hours. SAXS profiles after the annealing at 155°C is shown in Figure 2-4 (b) and we found that  $q/q_m = 1.22$ , suggesting that L is transformed into *Fddd* by annealing at 155°C. Finally, we cooled the sample to L region or 115°C where L is stable and annealed the sample at 115°C for 10 hours. SAXS profiles after annealing at 115°C in Fig 2-4 (c) has the peaks at  $q/q_m = 1$  and 2, indicating that L structure is recovered from *Fddd* structure after annealing at 115°C. Thus, the thermoreversibility exists between L and *Fddd*. These results confirmed that the *Fddd* region exists as an equilibrium phase in PS-rich region.

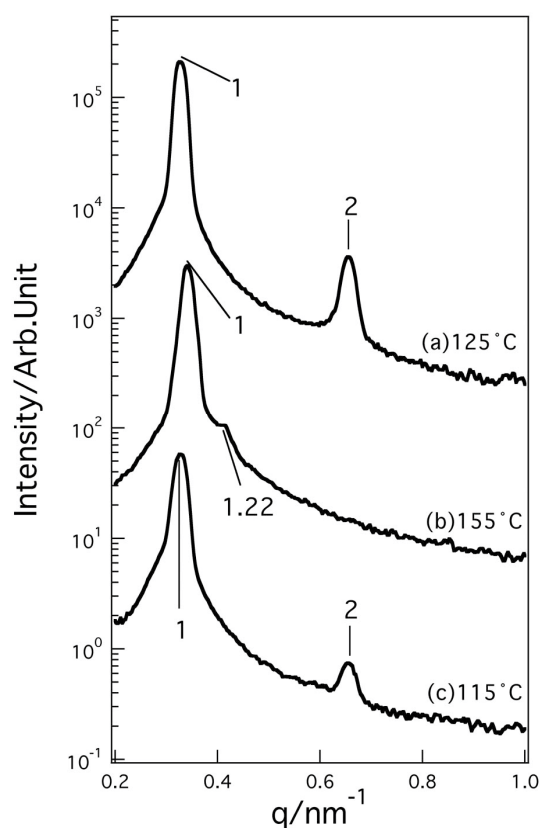


**Figure 2-4.** SAXS profiles of I3 ( $f_{PI} = 0.373$ ) after each step during thermal protocol: (a) after annealing at 125°C for 24 hours, (b) after annealing at 155°C for 20 hours, (c) after annealing at 115°C for 3 hours.

While  $Fddd$  structure exhibited in I2 and I3,  $Fddd$  phase was not observed in the other samples. Figure 2-5 shows the temperature dependence of SAXS profiles of I5 which has largest PI,  $f_{PI} = 0.385$ , in the sample. The peaks appeared at  $q/q_m=1, 2, \text{ and } 3$ , which indicates that I6 has L structure for all temperatures in ordered state except  $180^\circ\text{C}$ .

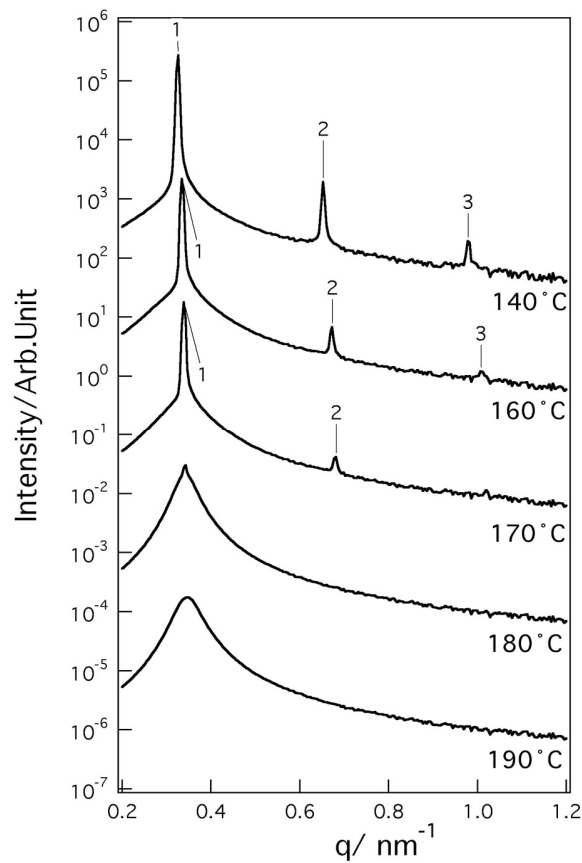


**Figure 2-5.** Temperature dependence of SAXS profiles for I5 ( $f_{PI} = 0.385$ ).

Temperature dependence of the SAXS profile for the lowest composition in SI diblock copolymer series,  $f_{PI} = 0.367$ , was shown in Figure 2-6. Distinct peak position at 1, 2, 3, and 4 indicates lamellar structure was formed at 120°C. As temperature increased, lamellar structure transformed into gyroid structure since SAXS profile has peaks located at  $q/q_m = 1, 1.15, 1.52, 1.9, 2.58, \text{ and } 2.9$ , which agree with those calculated for the gyroid structure.

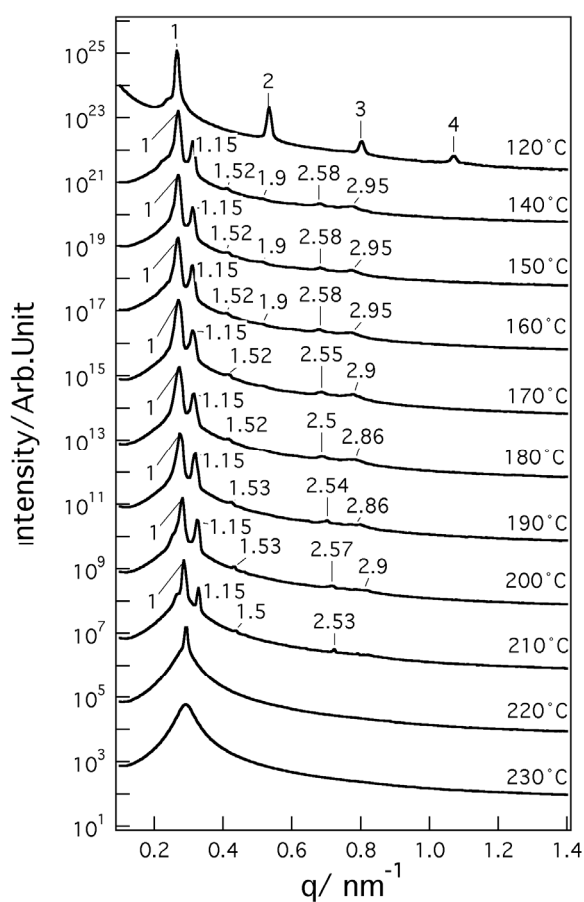


**Figure 2-6.** Temperature dependence of SAXS profiles for I1 ( $f_{PI} = 0.367$ ).

We determined the phase boundary of *Fddd* phase of SI diblock copolymer in PS-rich region in terms of  $f_{PI}$  and temperature. To eliminate the effects of molecular weight on the phase boundary, we plotted our identified phases in parameter space of  $\chi N$  on  $f_{PI}$ , instead of temperature on  $f_{PI}$ . To convert temperature to  $\chi$ , we employed the following relation by Khandpur et al.<sup>2</sup>:

$$\chi = 71.4/T - 0.0857. \quad (2)$$

Figure 2-7 shows the phase boundary of the *Fddd* phase in PS-rich region. Compared to the *Fddd* region in PI-rich region, the *Fddd* region in PS-rich region is much narrower than that in PI-rich region in the parameter space of  $\chi N$  on  $f_{PI}$  (Figure 2-8). In the case of PI-rich region, the *Fddd* phase extends to  $0.629 \leq f_{PI} \leq 0.649$  and  $25.6 < \chi N < 29.8$ . On the other hand, the *Fddd* phase in PS-rich region appears at  $0.37 \leq f_{PI} \leq 0.373$  and  $19.5 < \chi N < 21.1$ . Besides, the location of the *Fddd* phase in PS-rich region is not symmetric to that in PI-rich region in terms of  $\chi N$  and  $f_{PI}$ . The *Fddd* phase in PS-rich region is shifted to smaller  $\chi N$  values and is located closer to  $f_{PI} = 0.5$  than that in PI-rich region. The phase diagram is conventionally dictated using  $\chi N$  and  $f$ , while assuming both segments to be conformationally symmetric. However, since competition between stretching penalty of A and B blocks determines the microstructure, conformational asymmetry can have an effect on the phase diagram and phase boundaries.

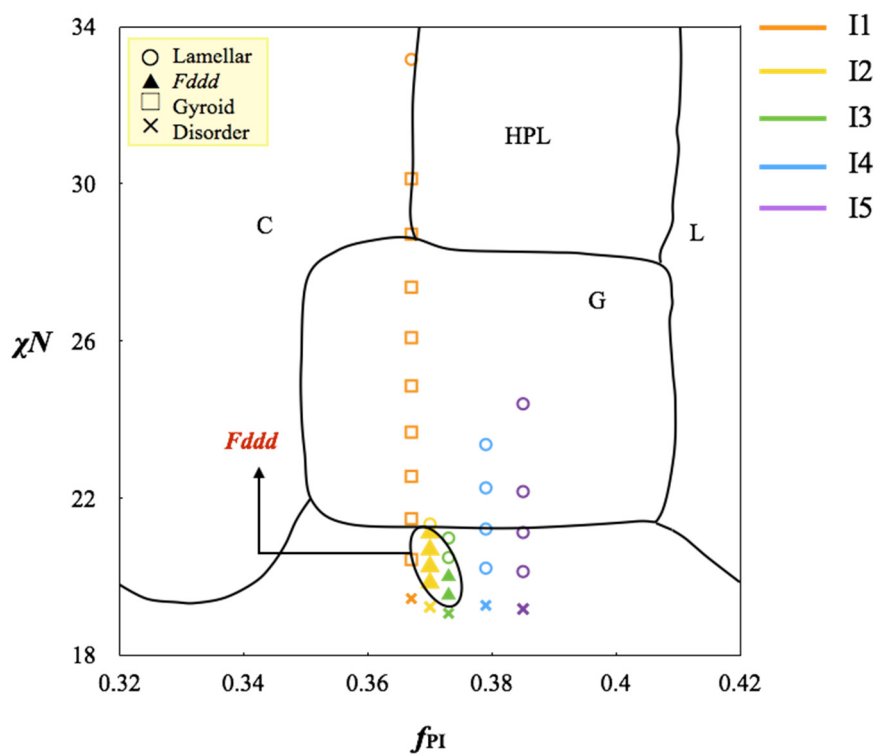


**Figure 2-7.** The phase boundary of the *Fddd* phase in PS-rich region. Solid line corresponds to the phase boundary determined by Khandpur et al<sup>2</sup>.

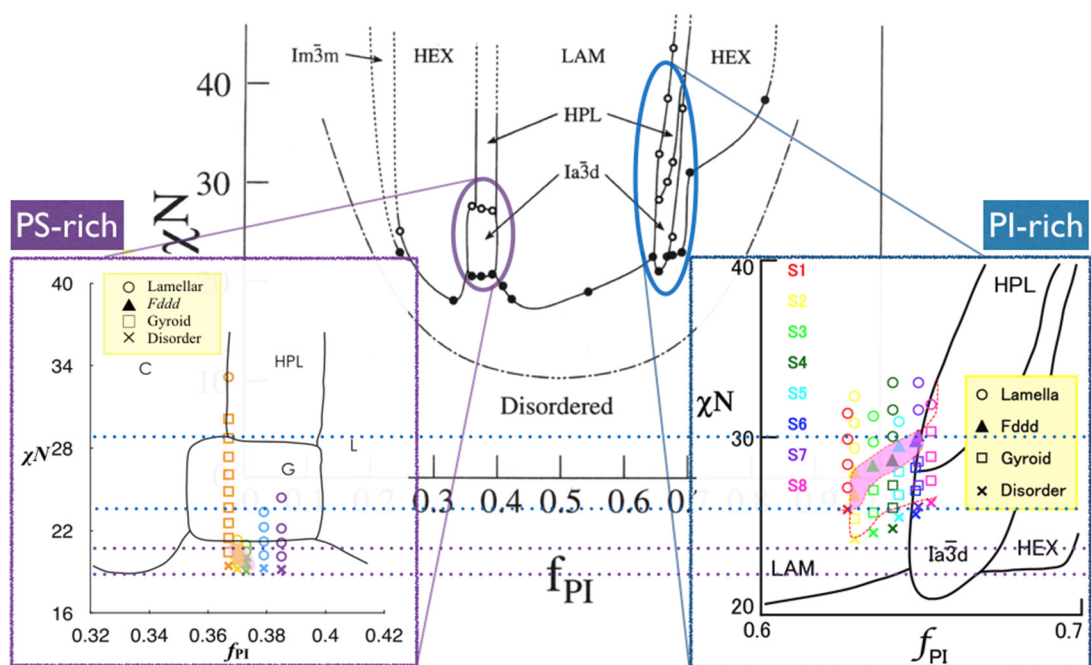


**Figure 2-8.** The phase boundary of the  $Fddd$  phase in PS-rich region and PI-rich region.

Recently, Matsen has developed a new scheme of self-consistent-field theory to calculate the phase diagram for block copolymers precisely<sup>11</sup>. He calculated the phase diagram of AB diblock copolymers with the scheme including the effects of conformational asymmetry and found that conformational asymmetry strongly affects the location of each phases in the parameter space of  $\chi N$  and  $f_{PI}$ . According to the phase diagram calculated for  $a_A/a_B = 1.5$ , the *Fddd* region in A-rich region extends to high  $\chi N$  region and is biased to  $f_A = 0.5$  while the *Fddd* region in B-rich region shift to  $f_A = 0.5$  and stay in lower  $\chi N$  region than that in A-rich region, where  $a_i$  is a statistical segment length of i-component. This tendency agrees with our results qualitatively. Theoretical calculations demonstrated that conformational asymmetry has a profound influence on order-order transitions (OOTs). The conformational asymmetry of SI diblock copolymer has been reported to be  $a_{PI}/a_{PS} = 1.22$ , thus we can concluded the conformational asymmetry causes the *Fddd* region in SI diblock copolymer to be asymmetric.

In addition to conformational asymmetry, thermal concentration fluctuations also affect to the phase boundary of *Fddd* structure<sup>12</sup>. In this work, we observed that the *Fddd* structure exists between the L and disorder phases in PS-rich region of SI diblock copolymers. Unlike the transition sequences found in PI-rich side (L-*Fddd*-G-Disorder)<sup>9</sup>, these SI diblock copolymers with PS-rich region showed L-*Fddd*-Disorder transitions with increasing temperature. Thermal fluctuation effects was considered as a possible reason for the direct transition from *Fddd* region to disordered state.

Observation of *Fddd* network as an equilibrium phase both in PS-rich and PI-rich region of SI diblock copolymers contradicts the prediction by Miao and

Wickham<sup>13</sup>, where they calculated the stability of *Fddd* phase in diblock copolymers under the effects of thermal fluctuations and found *Fddd* phase is metastable with respect to L and disorder phases. The contradiction may arise from the fact that the calculations of the effects involve a considerable number of approximations.

## 2-4. Conclusions

We investigated the phase behaviors of five SI diblock copolymers in PS-rich region, with different volume fraction of PI ranging from  $0.367 \leq f_{PI} \leq 0.385$  by the technique of SAXS and TEM. The *Fddd* structure survived after long-time annealing process, and the thermoreversibility in the OOTs between L and the *Fddd* structures was confirmed, indicating that *Fddd* structure exists as an equilibrium phase. The *Fddd* phase in PS-rich region is much narrower than that in PI-rich region, in the parameter space of  $f_{PI}$  and  $\chi N$ . The  $\chi N$  range of the *Fddd* phase in PS-rich region is shifted to lower  $\chi N$  than that in PI-rich region. The asymmetry of the *Fddd* phase in PS-rich rich regions agrees with the phase diagram calculated with self-consistent field theory including the effects of conformational asymmetry by Matsen, indicating that the conformational asymmetry causes the asymmetry of the *Fddd* phase in the phase diagram of SI diblock copolymers.

*Fddd* phase was firstly found in triblock copolymer melts by Bailly et al.<sup>14</sup>. We found the *Fddd* phase and Matsen et al. predicted the existence of *Fddd* phase in a wide

range of other block copolymer architectures<sup>15</sup>. These facts suggest that the *Fddd* phase could end up being a common phase among block copolymer systems.

## Reference

1. Matsen, M. W.; Schick, M. *Phys. Rev. Lett.* **1994**, 72, 2660-2663.
2. Khandpur, A. K.; Forster, S.; Bates, F. S.; Hamley, I. W.; Ryan, A. J.; Bras, W.; Almdal, K.; Mortensen, K. *Macromolecules* **1995**, 28, 8796-8806.
3. Hajduk, D. A.; Takenouchi, H.; Hillmyer, M. A.; Bates, F. S.; Vigild, M. E.; Almdal, K. *Macromolecules* **1997**, 30, 3788-3795.
4. Tyler, C. A.; Morse, D. C. *Phys. Rev. Lett.* **2005**, 94, 208302/1-208302/4.
5. Yamada, K.; Nonomura, M.; Ohta, T. *J. Phys.: Condens. Matter* **2006**, 18, L421-L427.
6. Ranjan, A.; Morse, D. C. *Phys. Rev. E* **2006**, 74, 011803.
7. Takenaka, M.; Wakada, T.; Akasaka, S.; Nishitsuji, S.; Saijo, K.; Shimizu, H.; Kim, M. I.; Hasegawa, H. *Macromolecules* **2007**, 40, 4399-4402.
8. Kim, M. I.; Wakada, T.; Akasaka, S.; Nishitsuji, S.; Saijo, K.; Hasegawa, H.; Ito, K.; Takenaka, M. *Macromolecules* **2008**, 41, 7667-7670
9. Kim, M. I.; Wakada, T.; Akasaka, S.; Nishitsuji, S.; Saijo, K.; Hasegawa, H.; Ito, K.; Takenaka, M. *Macromolecules* **2009**, 42, 5266-5271.
10. Jung, J.; Park, H.W.; Lee, J.; Huang, H.; Chang T.; Rho, Y.; Ree, M.; Sugimori, H.; Jinnai, H. *Soft Matter* **2011**, 7, 10424-10428.
11. Matsen, M. W. *Eur. Phys. J. E* **2009**, 30, 361-369
12. Bates, F. S.; Rosedale, J. H.; Fredrickson, G. H. *J. Chem. Phys.* **1990**, 92,

6255-6270.

13. Miao, B.; Wickham, R. A. *J. Chem. Phys.* **2008**, 128, 054902/1-054902/5.
14. Bailey, T. S.; Hardy, C. M.; Epps, T. H.; Bates, F. S. *Macromolecules* **2002**, 35, 7007-7017.
15. Matsen, M. W. *Macromolecules* **2012**, 45, 2161-2165.



## ***Chapter 3***

### ***Fddd* Structure in Polystyrene-*block*-polyisoprene Diblock Copolymer/ Polystyrene Homopolymer Blends**

#### **3-1. Introduction**

In chapter 2, we confirmed the stability of *Fddd* structure and found *Fddd* structure exists as an equilibrium structure in neat SI diblock copolymers in both side of phase diagram<sup>1-4</sup>. Previous studies reported that blending homopolymer with diblock copolymer causes order-order transition<sup>5-10</sup>. It is anticipated that diblock copolymer/homopolymer blend exhibits *Fddd* structure. In this study, we, hence, investigated the phase behaviors of SI diblock copolymer (SI)/ PS homopolymer (hPS) blends by small-angle X-ray scattering (SAXS) and transmission electron microscopy (TEM) and explored how blending homopolymer affects the *Fddd* region.

## 3-2. Experimental Section

The SI diblock copolymer samples were synthesized via living anionic polymerization in benzene at 50°C under an argon environment *sec*-BuLi was used as an initiator. The number-average molecular weight ( $M_n$ ) and polydispersity index (PDI) of SI diblock copolymer were determined by using size exclusion chromatography (SEC) using polystyrene standards. Volume fraction of polyisoprene ( $f_{PI}$ ) was determined by using  $^1\text{H}$  nuclear magnetic resonance (NMR) spectroscopy. We also identified that polyisoprene has a high degree of 1,4-addition (more than 95%) and a small degree of 3,4-addition (less than 5%) by NMR. hPS was purchased from TOSOH Corporation. The characterizations of the samples are listed in Table 3-1. We prepared the films of neat SI and four blend samples (B1~B4) by casting 5 wt% polymer solution in toluene with 0.2 wt% 2,6-di-*tert*-butyl-4-methylphenol as an anti-oxidant agent at 30°C for 1 week. The blend ratios of the four samples are listed in Table 3-2. The cast films were further dried at room temperature in vacuum for 1 day.

**Table 3-1.** Molecular Characteristics of SI and hPS.

Code	$M_n (\times 10^4) (\text{g} \cdot \text{mol}^{-1})$	$f_{PI}$	$M_w/M_n$
SI	26.1	0.651	1.01
hPS	5.73	-	1.02

**Table 3-2.** Characteristics of Blend Samples.

Code	SI/hP (wt./wt.)	$f_{PI}$
B1	99.2/0.8	0.646
B2	98.4/1.6	0.641
B3	97.6/2.4	0.636
B4	95.9/4.1	0.627

### 3-3. Results and Discussion

Figure 3-1 (a) shows the temperature dependence of SAXS profiles of the neat SI ( $f_{PI} = 0.651$ ) diblock copolymer. The scattered intensity  $I(q)$  is plotted as a function of wave number  $q$  ( $q = (4\pi/\lambda)\sin(q/2)$ ;  $q$  is scattering angle and  $\lambda$  is wavelength). At 165°C, the SAXS profiles exhibits a single broad peak indicating that the neat SI is in the disordered state. Below 165°C, several peaks are found in the SAXS profiles and the neat SI is in its ordered state. At 120 and 125°C, the peaks appear at  $q/q_m = 1, 2,$  and  $3$  in the SAXS profiles, where  $q_m$  is  $q$  at first-order peak. These integer multiples of peak position indicates that the lamellar structure (L) was formed at 120 and 125°C. As shown in Figure 3-2 (a), the striped pattern in TEM image at 120°C also suggests the lamellar structure. On the other hand, at 130 and 140°C, the ratios of  $q/q_m$  become different from those of the lamellar structure. The SAXS profiles at have peaks located at  $q/q_m = 1, 1.15, 1.82, 1.91, 2, 2.08, 2.52,$  and  $2.90$ , and agree with those of the gyroid structure (G) and the TEM image shown in Figure 3-2 (b) exhibits a 4-fold gridlike pattern, which is typical of the projection of a double-gyroid structure onto the (001) plane, in agreement with the SAXS result. Thus, the neat SI shows L-G-Disorder with increasing temperature and does not have *Fddd* region.

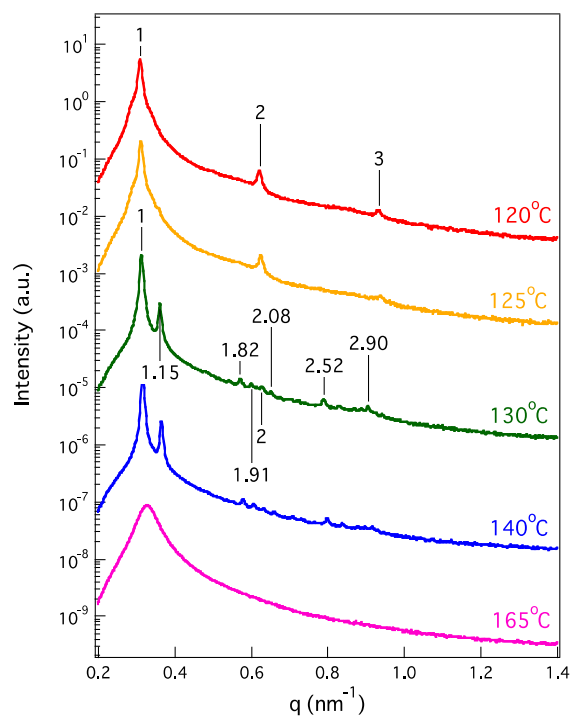


**Figure 3-1.** Temperature dependence of SAXS profiles for neat SI ( $f_{PI} = 0.651$ ). The profiles are shifted vertically to avoid overlapping.

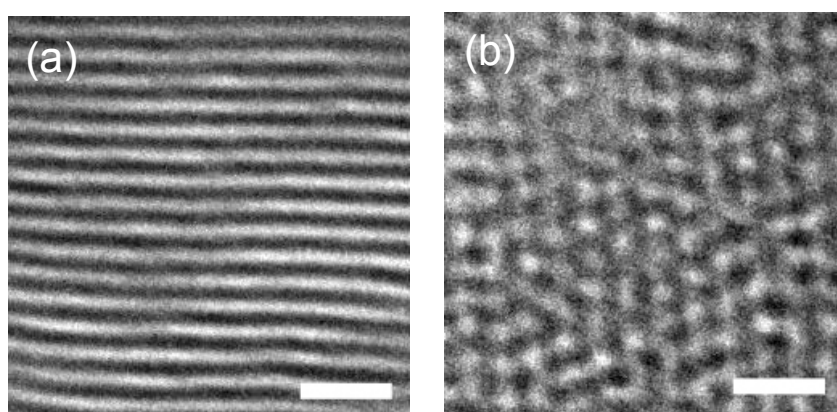


**Figure 3-2.** TEM images of neat SI at (a) 120°C and (b) 140°C. Dark region corresponds to PI. White scale bar corresponds to 50nm.

The temperature dependence of the SAXS profiles for the blend sample B1 ( $f_{PI} = 0.646$ ) is shown in Figure 3-3. At lower temperature or 100 to 125°C, the peak ratios become 1, 2, and 3 and L is stable. At 130°C, the scattering profile does not show multiple integer peak ratios. The SAXS peaks are located at  $q/q_m = 1, 1.22, 1.55, 1.72, 1.81, 1.95, \text{ and } 2.00$  with  $q_m = 0.344 \text{ nm}^{-1}$ , agreeing with the peak ratio of the *Fddd* structure as identified in SI diblock copolymer previously<sup>4</sup>. This fact suggests that the blend of hPS with SI can induce the order-order transition from G to *Fddd* at 130°C. The peaks can be indexed as 111, 004 ( $q/q_m = 1$ ), 113 (1.22), 115 and 131 (1.55), 133 (1.72), 202 (1.81), 222 (2.00). We estimated (a:b:c) = (1:2.08:3.62) with a = 20.7 nm by using

$$q_{hkl} = 2\pi[h^2/a^2 + k^2/b^2 + l^2/c^2]^{1/2}, \quad (1)$$

where a, b, and c are unit cell parameters and  $h, k, \text{ and } l$  are Miller indices for a, b, and c, respectively. At 135°C, the SAXS profile the peaks at  $q/q_m = 1, 1.15, 1.91, 2.52, 2.77, \text{ and } 2.90$  with  $q_m = 0.306 \text{ nm}^{-1}$ . These ratios agree with that of a double-gyroid structure. Thus, we found L-*Fddd*-G order-order transition with increasing temperature in B1 blend.

Similar to B1, B2 and B3 also have *Fddd* phase and exhibit L-*Fddd*-G order-order transition with increasing temperature. Figures 3-4 shows the temperature dependence of SAXS profiles of B3 ( $f_{PI} = 0.636$ ). *Fddd* phase are found at 145 to 150°C in B3 between L and G phases. Though we do not show here, B2 is also found to have

*Fddd* phase at 135 to 140°C between L and G phases. The *Fddd* regions shift toward higher temperature with  $f_{PI}$ , which agrees with the tendency of the *Fddd* phase of the neat SI.

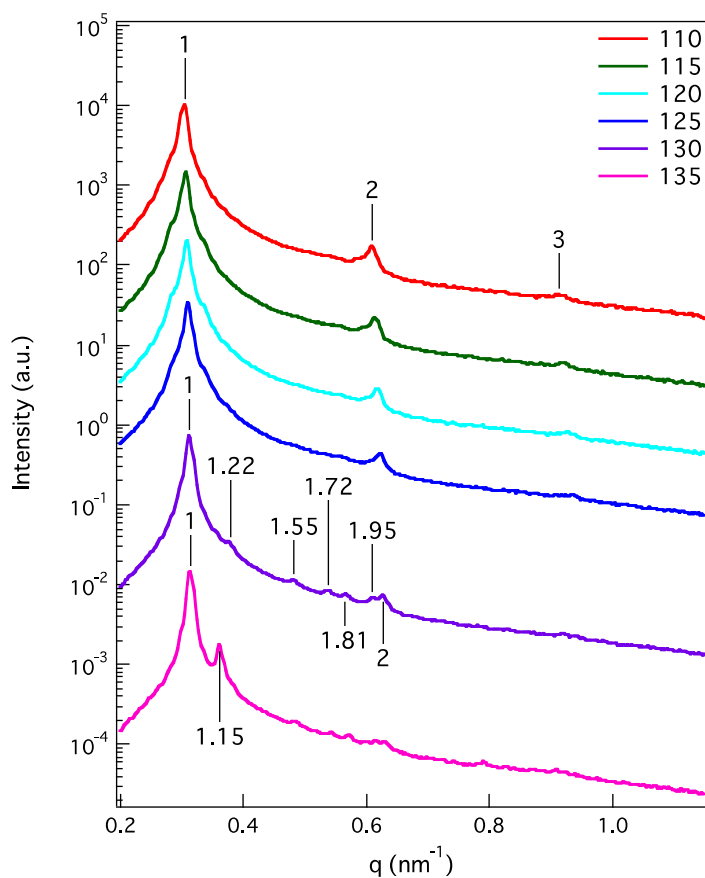


**Figure 3-3.** Temperature dependence of SAXS profiles for B1 ( $f_{PI} = 0.646$ ). The profiles are shifted vertically to avoid overlapping.

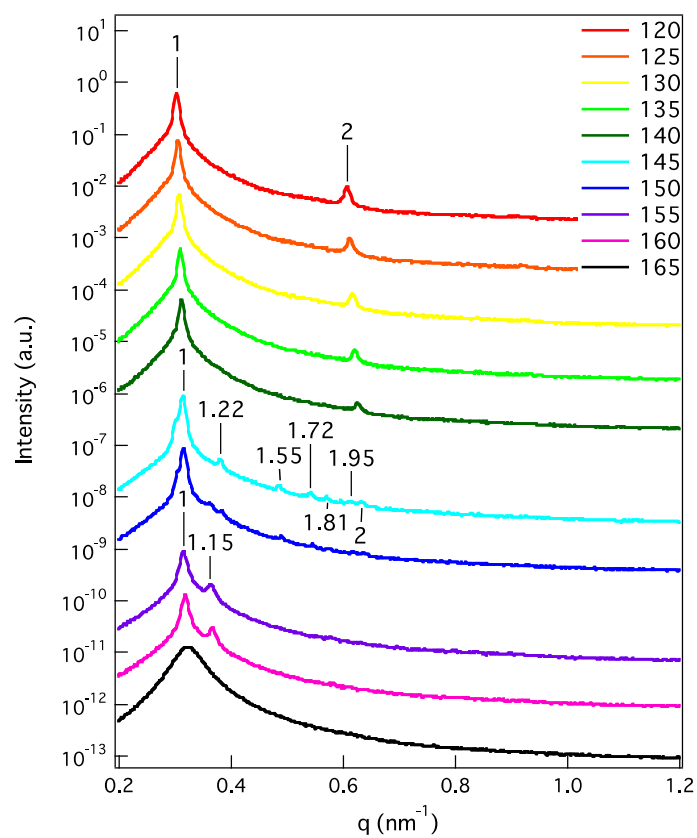


**Figure 3-4.** Temperature dependence of SAXS profiles for B3 ( $f_{PI} = 0.636$ ). The profiles are shifted vertically to avoid overlapping.

While  $Fddd$  structure exhibited in B1, B2, and B3,  $Fddd$  phase was not observed in B4. Figure 3-5 shows the temperature dependence of SAXS profiles of B4 ( $f_{PI} = 0.627$ ). For all measurement temperatures except 164°C, the peaks in the SAXS profiles appeared at peak ratios of 1, 2, and 3, thus, the sample forms lamellar structure in its ordered state. At 164°C, a single broad peak appeared, which means the disordered state. Even though there is a very small difference in the volume fraction of polyisoprene between B3 and B4, B4 did not exhibit  $Fddd$  and gyroid structure.

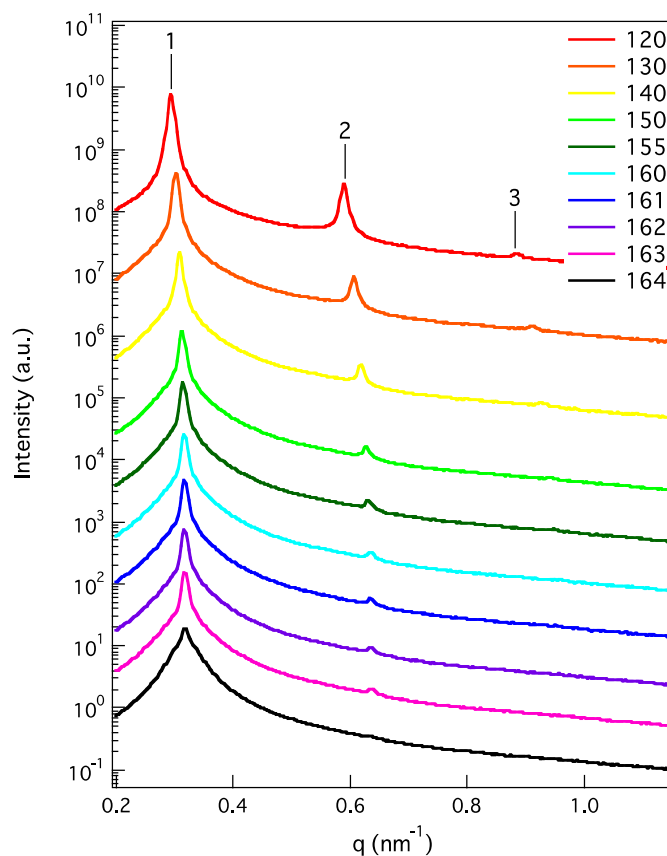


**Figure 3-5.** Temperature dependence of SAXS profiles for B4 ( $f_{PI} = 0.627$ ). The profiles are shifted vertically to avoid overlapping.

We determined the phase boundary of *Fddd* phase of SI/ hPS blends in terms of  $f_{PI}$  and temperature. To compare the phase boundary of the blends with that of the neat SI, we plotted our identified phases in parameter space of  $\chi N$  on  $f_{PI}$ , instead of temperature on  $f_{PI}$ , where  $N$  is the polymerization index of SI. To convert temperature to  $\chi$ , we employed the following relation by Khandpur et al.<sup>11</sup>:

$$\chi = 71.4/T - 0.0857. \quad (2)$$

Figure 3-6 shows the phase boundary of the *Fddd* phase of SI/ hPS blends. The *Fddd* region of the blends extends to  $0.632 \leq f_{PI} \leq 0.641$  and  $27.5 < \chi N < 30.2$ . Compared to the *Fddd* region of the blends with the *Fddd* region of the neat SI, Both regions are almost identical.

Hong, Whitmore and Noolandi<sup>5, 6</sup> have discussed the effects of the addition of homopolymer on the phase diagram of the block copolymer. According to their theory, The critical point of the diblock copolymer/ homopolymer blends  $(\chi N)_{C, Blend}$  is expressed by

$$(\chi N)_{C, Blend} = 10.5 + 10.5 \left[ 1 + 5.25 \left( \frac{N_H}{N} \right) g(x^*) \right] \phi_H \quad (3)$$

where  $N_H$  and  $\phi_H$  are, respectively, the polymerization index and the volume fraction of homopolymer.  $g(x^*)$  is given by

$$g(x^*) = \frac{1 - e^{-x^*}}{x^*} \quad (4)$$

with

$$x^* = 3.78(N_H/N) \quad (5)$$

Substituting  $N = 336$ ,  $N_H = 55$ , and  $\phi_H = 0.04$  (corresponding to B4) into eqs. (3) to (5),  $(\chi N)_{C, \text{Blend}}$  is estimated as 10.45 so that the addition of the homopolymer does not affect the critical point in our experiment condition.

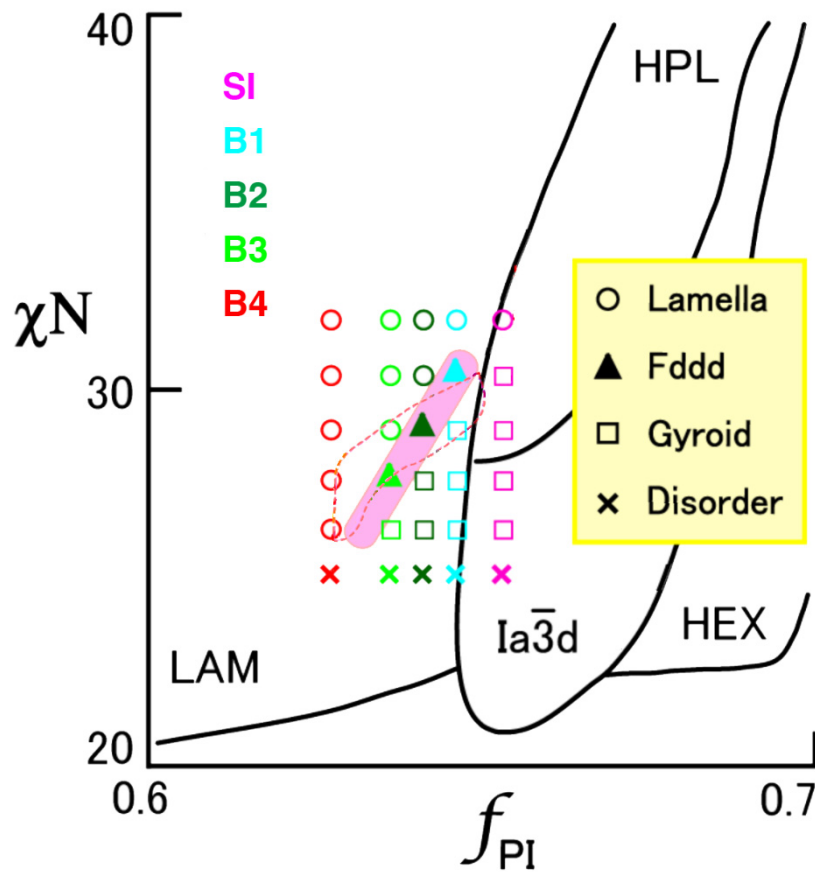


**Figure 3-6.** The phase boundary of the  $Fddd$  phase of SI/ hPS blends. Broken line corresponds to the phase boundary of the neat  $SI^3$ .

Although the equations are introduced for symmetric block copolymers or  $f = 0.5$ , the asymmetry in our case ( $f \sim 0.6$ ) does not alter the tendency obtained by the equations. The coefficients of the free energy density function would also not be changed significantly by the addition of homopolymer in our case<sup>10</sup>. Thus, the addition of homopolymer in our case does not affect the phase region of *Fddd* and the *Fddd* phase region of the blends is well superimposed into that of the neat SI.

### 3-4. Conclusions

We have induced *Fddd* structure in SI diblock copolymer which does not have *Fddd* phase by adding hPS. We prepared the SI/ hPS blend samples in the range of  $0.627 < f_{PI} < 0.646$  and investigated the phase boundary of *Fddd* phase by using small-angle X-ray scattering (SAXS) and transmission electron microscope (TEM) where  $f_{PI}$  is volume fraction of polyisoprene (PI) in SI/ hPS. We found the *Fddd* phase as an equilibrium phase in the range of  $0.632 \leq f_{PI} \leq 0.641$  and  $27.5 < \chi N < 30.2$ , where  $\chi$  and  $N$  are, respectively, the Flory-Huggins interaction parameter between PS and PI, and polymerization index of the diblock copolymer. The *Fddd* phase boundary in the SI/ hPS is similar to that in the neat SI block copolymer. This is because the addition of the homopolymer does not affect the critical point in our experiment condition.

## Reference

1. Takenaka, M.; Wakada, T.; Akasaka, S.; Nishitsuji, S.; Saijo, K.; Shimizu, H.; Kim, M. I.; Hasegawa, H. *Macromolecules* **2007**, *40*, 4399-4402.
2. Kim, M. I.; Wakada, T.; Akasaka, S.; Nishitsuji, S.; Saijo, K.; Hasegawa, H.; Ito, K.; Takenaka, M. *Macromolecules* **2008**, *41*, 7667-7670.
3. Kim, M. I.; Wakada, T.; Akasaka, S.; Nishitsuji, S.; Saijo, K.; Hasegawa, H.; Ito, K.; Takenaka, M. *Macromolecules* **2009**, *42*, 5266-5271.
4. Wang, Y. C.; Matsuda, K.; Kim, M. I.; Miyoshi, A.; Akasaka, S.; Nishitsuji, S.; Saijo, K.; Hasegawa, H.; Ito, K.; Hikima, T.; Takenaka, M. *Macromolecules* **2015**, *48*, 2211-2216.
5. Hong, K. M.; Noolandi, J. *Macromolecules* **1983**, *16*, 1093-1101.
6. Whitmore, M. D.; Noolandi, J. *Macromolecules* **1985**, *18*, 2486-2497.
7. Tanaka, H.; Hashimoto, T. *Polym. Commun.* **1988**, *29*, 212-216
8. Hashimoto, T.; Tanaka, H.; Hasegawa, H. *Macromolecules* **1990**, *23*, 4378-4386.
9. Tanaka, H.; Hasegawa, H.; Hashimoto, T. *Macromolecules* **1991**, *24*, 240-251.
10. Ranjan, A.; Morse, D. C. *Phys. Rev. E* **2006**, *74*, 011803.
11. Khandpur, A. K.; Forster, S.; Bates, F. S.; Hamley, I. W.; Ryan, A. J.; Bras, W.; Almdal, K.; Mortensen, K. *Macromolecules* **1995**, *28*, 8796-8806.



## *Chapter 4*

### **3D-TEM Study on the Morphology of PS-*b*-(PVPDVS-*g*-PI) Block-Graft Copolymer**

#### **4-1. Introduction**

Block copolymers are capable of forming periodic structures such as lamellae, *Fddd*, gyroid, hexagonally-packed cylinder, and sphere. The chemical junctions connect immiscible chains at the interface between separated microdomains allow the phase separation occur in a microscopic scale of 5 - 100 nm. The thermodynamic balance between the conformational entropy loss and the interfacial energy increase dictates the microphase separation behaviors below order-disorder transition<sup>1-3</sup>. Increasing or decreasing block copolymer composition, away from the symmetric condition introduces a spontaneous curvature, and ordered-ordered phase transition from lamellae to hexagonally-packed cylinder to sphere occurs.

In addition to volume fraction, molecular architecture also affect the morphology of block copolymers. Relationship between molecular architecture and morphology has been studied systematically for diblock and triblock copolymers<sup>4-7</sup>, but few studies have been investigated for graft copolymers due to the unavailability of well-defined graft copolymers<sup>8-10</sup>.

The objective of this study is thus to examine the bicontinuous morphology of polystyrene-*block*-(poly-4-vinylphenyldimethylvinylsilane-*graft*-polyisoprene), PS-*b*-(PVPDVS-*g*-PI), block-graft copolymer that has well-defined arrangement of grafts. Accurate classification of the complex morphology such as the shape of the microdomains, especially the way of connection in the network microdomains relied upon transmission electron microscopy (TEM). However, by conventional TEM, we can only obtain the projections of three-dimensional structures onto a two-dimensional plane when identifying the complicated structures. On the other hand, three-dimensional images of the complex structures can be obtained by electron tomography based on the computed tomography (CT)<sup>11</sup>, which is a useful tool for analyzing the microdomain structures, grain boundaries in block copolymers. In this study, we investigated the bicontinuous structure in 3D real space by electron tomography to obtain reasonable 3D reconstructions.

## 4-2. Experimental Section

Polystyrene-*block*-(poly-4-vinylphenyldimethylvinylsilane) (PS-*b*-PVPDVS, code: SGI-2) were prepared via anionic living polymerization under an argon environment using sec-butyllithium as an initiator. Polymerization and the backbone coupling process were conducted in a sealed glass apparatus under pressure of  $10^{-5}$  mmHg. Polymerization techniques were reported and described elsewhere by Fujimoto et al.<sup>12</sup>, Se. K et al<sup>13, 14</sup>.

Number-average molecular weight ( $M_n$ ) and polydispersity index (PDI) of the backbone, graft and the block-graft copolymer were determined by gel permeation chromatography (GPC). For GPC measurement, THF was used as the eluent at 25°C.

The characterizations of the SIG-2 sample are listed in Table 4-1. Prior to each experiment, we made 5 wt% polymer solution in toluene with 0.2 wt% 2,6-di-tert-butyl-4-methylphenol as an anti-oxidant agent and then cast them at 30°C for 1 week. The cast films were further dried at room temperature in vacuum for 1 day. Thickness of the as-cast films is about 0.1mm.

**Table 4-1.** Molecular Characteristics of PS-*b*-(PVPDVS-*g*-PI) block-graft Copolymer.

	Polymer	$M_n (\times 10^5)(\text{g} \cdot \text{mol}^{-1})$	$f$
backbone	PS	2.4	0.54
	PVPDVS	0.1	-
grafts	PI	1.8	0.46

The film specimen of PS-*b*-(PVPDVS-*g*-PI) block-graft copolymer was prepared by casting 5 wt% benzene solution at room temperature. The cast-film was further dried at room temperature in vacuum for 1 day to attain the complete removal of solvent. Prior to TEM observation, the samples were microtomed into 120 nm thickness at -55°C using a Reichert-Nissei Ultracut S ultramicrotome equipped with a Leica EM FCS cryo kit. The ultrathin sections were collected and put on the copper grids covered by carbon-coated poly(vinyl formal) membrane. They were stained with OsO<sub>4</sub> for 1h. The TEM observation was performed using JEM-2000FX with the acceleration voltage being 200kV.

For electron tomography, which combines the computed (CT) technique with TEM<sup>11</sup>, tilt series TEM images were taken from the same specific area of the ultrathin section specimen. 61 TEM images was acquired at angles tilting from -60° to +60° in 2° increments. These obtained TEM images were aligned with respect to the gold fiducial markers. The reconstructed image was obtained by using the filtered-back-projection (FBP) method with IMOD program. We used the software Analyze 10 to analyze the obtained 3D image.

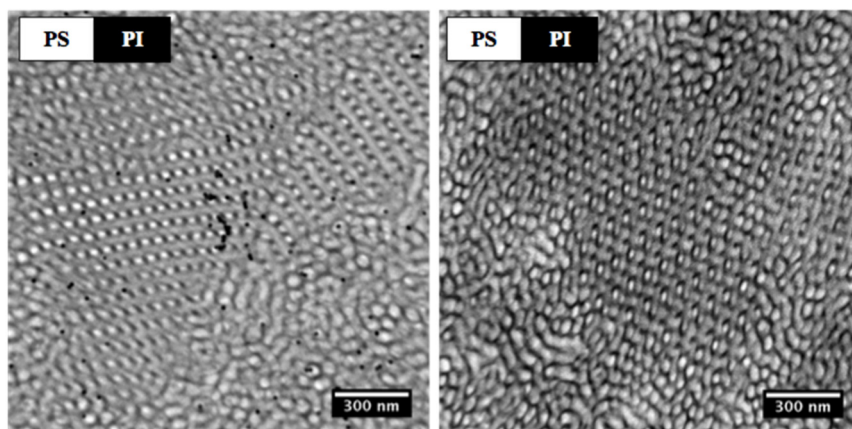
### 4-3. Results and Discussion

Figure 4-1 shows two-dimensional electron micrograph obtained from a ca. 120-nm-thick section of PS-*b*-(PVPDVS-*g*-PI) (sample code: SIG-2) block-graft copolymer films in different regions. The white area in the micrographs corresponds to the PS/PVS backbone phases, while the PI grafts are stained dark by the vapor of osmium tetroxide. The dark PI phase forms the matrix and the network structure consists of PS/PVS phases fills up the interstices of PI matrix, wherein the PS/PVS phase can be viewed as a mixed microdomain of PS and PVS blocks. It should be noticed that since the PVS content of SIG-2 bloc-graft copolymers is 1.7%, there is no particular consideration for the possible microphase structure of PVS in this study. It is obviously that the complicated structure in both figures is ordered and periodic over almost all the films although being mixed with irregular grains in some regions. The sponge-like morphology originates from the concentration fluctuations of disordered state as observed by Sakamoto et al. in SI diblock copolymers<sup>15</sup>.

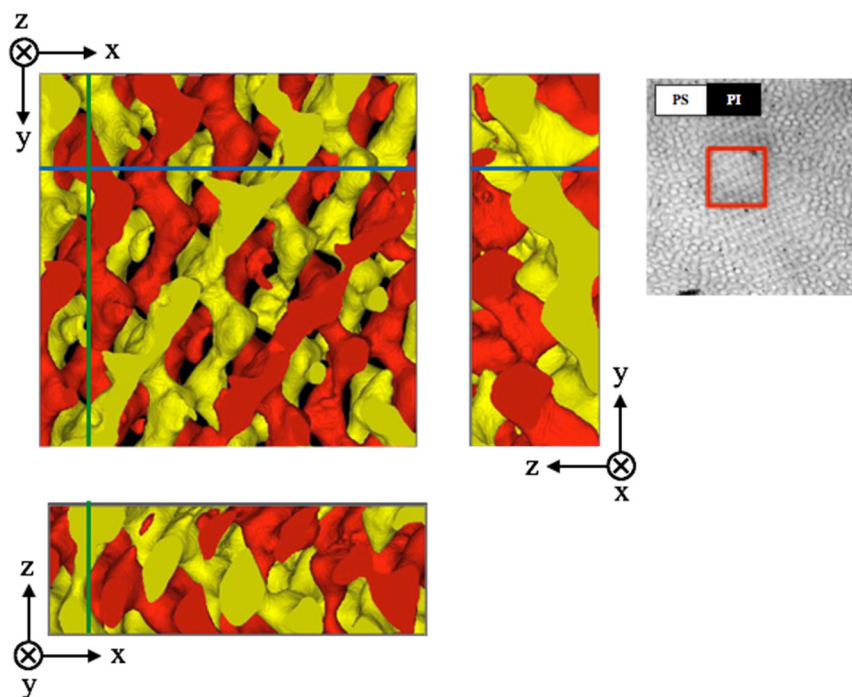
Figure 4-2 shows the 3D image reconstructed from the series of tilt TEM images. The planar and the cross-sectional slice images of the rendering three-dimensional volume elements are exhibited. For reference, we defined the z-axis as the direction of electron beam orthogonal to the specimen surface, and the xy plane is parallel to the surface. The color solids (red and yellow) correspond to the PS network domain. They are network domains but they are not connected each other. The two cross-section images indicate that the network is continuous over the three-dimension.

Figure 4-3 (a) demonstrates the selected OsO<sub>4</sub>-stained section of SIG-2 thin film. The PS network structure consists of two interpenetrating double network indicated in yellow and red color, and is embedded in PI matrix. Additionally, the double networks exhibit a six-membered ring structure (hexagon in Figure 4-3 (a)) and resemble the “wagon-wheel” image, which also has six radial arms. The morphological features of the 3D image are identical with those observed in OBDD.

We can separate the images of two networks into two images of each network as shown in Figure 4-3 (b) and Figure 4-3 (c). It is remarkably that image of Figure 4-3 (b) has exactly the same network structure as that of Figure 4-3 (c), indicating the two networks are identical. Further observation of the micrograph allows us to recognize that the structural unit consists of four rodlike elements joined together to form a regular tetrahedron (arrow in Figure 4-3 (b)). Thus it is concluded that the PI phase forms the matrix and fills with the interwoven bicontinuous structure of two sets of tetrapod networks of PS phase, and both the PI and PS phases are continuous in three dimensions. According to these results, the most probable model to interpret the double network structure of SGI-2 block-graft copolymer is a double-diamond lattice.



**Figure 4-1.** Electron micrographs of the network structure obtained in SGI-2 film cast from solution in benzene and were stained by OsO<sub>4</sub>.



**Figure 4-2.** Orthogonal digital slices of the 3D reconstructed image of planar (x,y) and cross-sectional (x,z) (y,z) image, where the yellow and red solid indicates the PS network microstructure and the PI matrix is adjusted to be transparent.

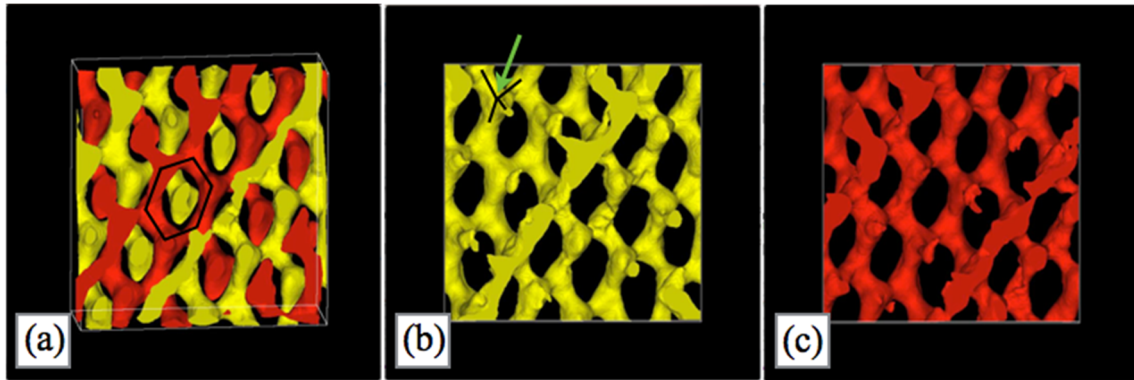


**Figure 4-3.** (a) Cross-sectional image in x, y plane, and (b) (c) isolated network of the double network structure separated from Figure 4-3 (a).

To check whether the characteristics of the morphology in 3D TEM image agree with those of the OBDD, we compared the structures of the 3D image with that of OBDD at several length scale, as shown in Figure 4-4. Firstly, we compared the elemental unit of the network. As shown in Figure 4-4 (a), both the experimental image and the OBDD model display a tetrapod consisting of four rodlike elements, and hence the same features. In larger scale as shown in Figure 4-4 (b), these tetrapod constituting units connect to each other and form a six-membered ring structure in both images. Three nodes of the six consecutive nodes point upward and another three nodes point downward direction normal to the surface in an alternating way. In the OBDD model,

the double networks are formed by two networks in 3D TEM images, and the tetrapod units of SIG-2 film exhibit double-diamond lattice when they assemble to form network structure in a three-dimensional space as well. These comparisons concluded unambiguously that OBDD is the most suitable candidate to represent the morphology, where OBDD network of PS phase embedded in the matrix of PI phase.

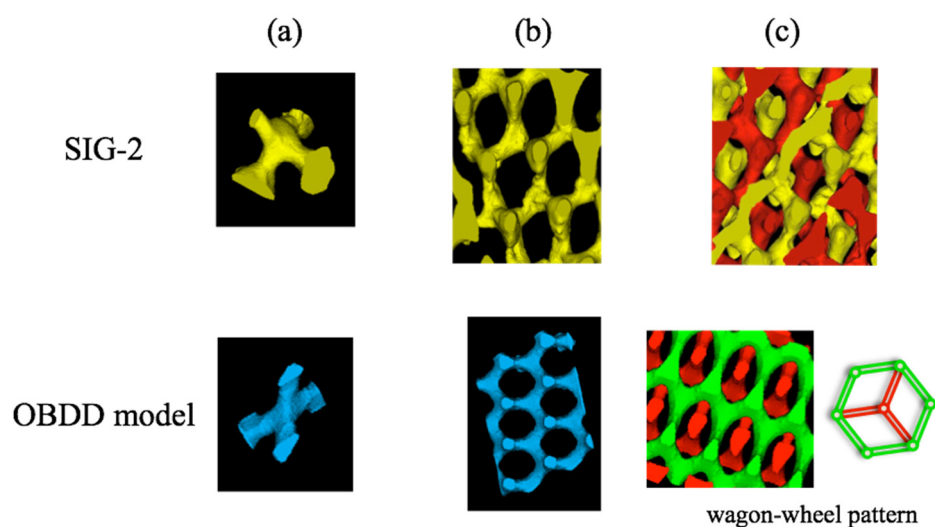


**Figure 4-4.** Comparisons of (a) constituting unit (structural unit), (b) six-membered ring structure and (c) double network of 3D reconstructed image between the double network structure reconstructed of SGI-2 cast film and OBDD model.

In the case of asymmetric diblock copolymer (i.e.  $f_A \neq f_B$ ), it is favorable for the domains between segments to have curved interface. The interface curvature of the typical block copolymer is shown in Figure 4-5 (a). In general, minor component would stay in the concave side of the interface and form the network part of the network structure embedded in the matrix consist of the major phase of copolymers. However, contrary to the general case, block with larger volume fraction, PS, forms the network phase and minor component PI becomes matrix phase in this study. The unique molecular architecture of SIG-2 block-graft that PI block connects with PVS-grafted PS could be responsible for the inverse microdomain structure. For each PS segment there are 10 PI grafts attach to the PVS block, which makes the PI become bulkier and thus forms the matrix phase even though PI has a smaller composition.

The SGI-2 film has a PS and PI content of 0.54 and 0.46, respectively. PS-*b*-PI diblock copolymer with the volume fraction of PS being 0.54 would form a lamellar structure. However, the SGI-2 film shows the OBDD network structure where major component PS forms the continuous network phase embedded in PI matrix phase. Packing frustration is responsible for the discrepancy in the phase behavior since PI graft chains and PVPDVS back bone chains emanate from a common junction point, the chains avoid chain stretching to achieve maximum conformational entropy and form a curved interface. In this particular block-graft copolymer, the PI chains have to stretch perpendicular to the interface to maintain the segmental density constant, which is thermodynamically unfavorable. In consequence, by curving the interface away from PI domains, the high stretching PI grafts can be alleviated. Thus, SGI-2 block-graft

copolymer results in a preference for PI grafts to remain on the convex side of the interface. This preference induces the shifts of order-order transition to higher PS volume fraction in phase diagrams.

Previously, Scott T. Milner reported the relationship between the chain architecture and asymmetry in copolymers<sup>16</sup>. It was shown in this study that a strong dependence of the phase boundary on the number of arms of diblock polymers. As the ratio of  $N_{\text{graft, PI}}/N_{\text{graft, PS}}$  increase (i.e. the number of PI grafts increase) the bicontinuous phase (bicB phase) will shift to the higher PS content side in the phase diagram. That is to say, OBDD network morphology is formed around symmetric composition if proper amount of graft is contained.

Finally, the schematic illustration of packing model of OBDD network structure in SGI-2 is displayed in Figure 4-5 (c). In the high interface curvature region, the interface area between PS and PI phase is expanded and form the upper part of the OBDD network lattice as shown in the left-hand side of Figure 4-5 (c). On the other hand, it is easier for polymer chains to stretch and the steric hindrance from the segments becomes lower since the graft chains are mixed in the low interface curvature region. The shorter block PI appears on the convex side of the interface while the longer block PS forms the minority component phase (OBDD network) on the concave side. The spatial arrangement of the PS and PI chains enable the network structure consists of PS phase to fill up the interstices of PI matrix and relieve packing frustration inside the tetrapod nodes, stabilizing the OBDD morphology. SIG-2 graft-block copolymer has different segmental density in PS and PI domains, which forces the PI grafts to deform

and accommodate the PS blocks and forms a curved interface between PS and PI domains. The formation of OBDD was attributed to the preferred interfacial curvature and packing density induced by the block-graft architecture of SGI-2.

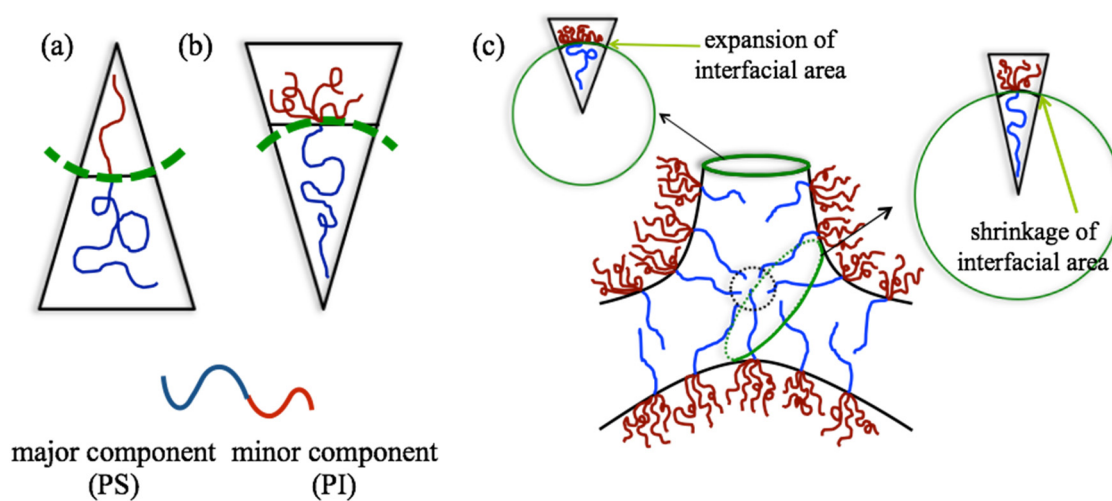


**Figure 4-5.** Schematic presentation of (a) interface curvature of common block copolymer, (b) interface curvature of SGI-2 in the presenting study and (c) the packing model of OBDD network structure in SGI-2.

## 4-4. Conclusions

The microdomain morphology of PS-*b*-(PVPDVS-*g*-PI) (SIG-2) block-graft copolymer with  $f_{PS} = 0.54$  in the film cast from benzene solutions is found to exhibit OBDD structure. According to the TEM analysis, the structural unit found for SIG-2 is a tetrahedral PS rod arranged and exhibits the symmetry of a diamond cubic lattice. The network structure consists of two mutually identical interwoven but unconnected three-dimensional networks of major PS segments embedded in the minor PI phase matrix. We consider the double-diamond lattice model is the most suitable to demonstrate the obtained microdomain structure. The effective volume fraction in the SIG-2 block-graft copolymer is an important factor of the resulting morphology. The bulky PI graft attached on the PS/PVS block copolymer on the amount of 10 branches per chain on averages stretch than the unperturbed polymer chain, and thus the SIG-2 forms OBDD network structure that is unusual to the common block copolymers.

## Reference

1. Meier, D. J. J. *Polym. Sci. Part C* **1969**, 26, 31.
2. Helfand, E.; Wasserman, Z. R. *Macromolecules* **1978**, 11, 960-966; **1980**, 13, 994-998.
3. Ohta, T.; Kawasaki, K. *Macromolecules* **1986**, 19, 2621-2632.
4. Molau, G. E., Aggarwal, S. L., Eds.; *Block Copolymers*; Plenum Press: New York, **1970**.
5. Norhay, A.; McGrath, J. E. *Block Copolymers*; Academic Press: New York, **1977**.
6. Shen, M.; Kawai, H. *AIChE J.* **1978**, 24, 1-20.
7. Kotaka, T., Ed.; Tokyo Kagaku Dohjin: *Polymer Alloy Tokyo*, **1993**.
8. Price, C.; Woods, W. *Polymer* **1973**, 14, 82-86.
9. Ito, K.; Usami, N.; Yamashita, Y. *Macromolecules* **1980**, 13, 216-221.
10. Rempp, P.; Franta, E.; Herz, J. *American Chemical Society: Washington, DC*, **1981**; p 59.
11. Frank, J., *Electron Tomography*. 2nd ed.; Springer: New York, **2005**.
12. Fujimoto, T.; Nagasawa, M. *Polym. J.* **1975**, 7, 397-401.
13. Se, K.; Kijima, M.; Fujimoto, T. *Polym. J.* **1988**, 20, 791-799.
14. Matsumura, K.; Ueda, K.; Se, K.; Fujimoto, T. *Polym. Prepr. Jpn.* **1984**, 33, 153.
15. Sakamoto, N.; Hashimoto, T. *Macromolecules* **1995**, 28, 6825-6834.
16. S.T. Milner. *Macromolecules* **1994**, 27, 2333-2335.

## ***Chapter 5***

### **The formation of OBDD Network Structure in PS-*b*-PI-*b*-PDMS Triblock Copolymer**

#### **5-1. Introduction**

ABC triblock copolymers consisting of mutually immiscible A, B and C polymer segments present various ordered structures compared to diblock copolymers<sup>1-6</sup>. An addition of C block to AB diblock copolymer provides richer geometry of the microdomain structures in ABC triblock copolymers, and the morphologies can be considered by a simple combination of spherical, cylindrical and lamellar shapes. In addition, complex equilibrium structures have been reported such as core-shell gyroid (Q<sup>230</sup>)<sup>7-10</sup>, *Fddd*<sup>11-14</sup> and alternating gyroid (Q<sup>214</sup>)<sup>15-18</sup> in ABC triblock copolymers.

In order to create more interesting and complex microdomain morphologies in block copolymers, self-assembly of non-equilibrium morphology through

non-equilibrium processes is required. Two-step phase separation during solvent cast process is one of the fascinating processes. For some ABC triblock copolymers, the three components will not segregate from each other simultaneously during casting process. In other words, one of the three components segregates first while the remaining two components are still miscible, which resembles the microphase separation in diblock copolymers. The other two components segregate in the second step within the pre-constructed microdomain that is formed in the first step of microphase-separation process. Microdomain morphology can thus be controlled via the two-step microphase separation when the system composed of more than three components. Polystyrene-*block*-polyisoprene-*block*-polydimethylsiloxane (SID) in toluene solution meets this condition since PS and PI are miscible in toluene while PDMS is less miscible in toluene. Thus, we anticipate that SID triblock copolymer has a two-microdomain structure in the first step, one phase consists of PS/PI disordered state and the other consists of the PDMS block. In the second step, the mixed PS and PI blocks microphase-separate into two phases.

In this study, we then investigated the morphology and the self-assembly process of SID cast from toluene solution. The result from electron microscopy and SAXS studies of the morphology shows non-equilibrium OBDD structure was found in triblock copolymer composed of SID with S/I/D volume fraction 0.284/0.36/0.356 and a molecular weight of 179,000 g/mol. The concentration dependence of SAXS profiles indicates the two-step microphase separation occurs during the self-assembly of SID in solvent cast process, resulting in the complex OBDD morphology.

The origin of the formation of non-equilibrium OBDD will also be discussed.

## 5-2. Experimental Section

Polystyrene-*block*-polyisoprene-*block*-polydimethylsiloxane (code: SID1) was synthesized via living anionic polymerization in benzene under an argon environment using *sec*-BuLi as an initiator. Number-average molecular weight ( $M_n$ ) and polydispersity index (PDI) of SID1 triblock copolymers were determined by membrane osmometry in toluene at 35 °C and size exclusion chromatography in THF at 30 °C, respectively. Volume fraction of polystyrene, polyisoprene and polydimethylsiloxane ( $f_{PS}$ ,  $f_{PI}$  and  $f_{PDMS}$ ) were determined by using  $^1\text{H}$  nuclear magnetic resonance (NMR) spectroscopy. The characterizations of the samples are listed in Table 5-1. Prior to each experiment, we made 5 wt% polymer solution in toluene and then cast them at 25°C for 1 week. The cast films were further dried at room temperature in vacuum for 1 day. Thickness of the as-cast films is about 0.1 mm. In order to investigate the self-assembly process during casting, we prepared several toluene solutions of SID1 with different concentrations.

**Table 5-1.** Molecular Characteristics of SID1 Triblock Copolymer.

Code	$M_n (\times 10^5) (\text{g} \cdot \text{mol}^{-1})^a$	$f_{\text{PS}}^b$	$f_{\text{PI}}$	$f_{\text{PDMS}}$	$M_w/M_n^c$
SID1	1.79	0.284	0.36	0.356	1.05

<sup>a</sup> Membrane osmometry in toluene at 35 °C. <sup>b</sup> <sup>1</sup>H NMR in CDCl<sub>3</sub> at 20 °C. <sup>c</sup> Size exclusion chromatography in THF at 30 °C.

Synchrotron SAXS experiments were performed at BL45XU in SPring-8 to examine the morphologies of the cast film and the solution. At BL45XU, the wavelength and the sample-to-detector distance are, respectively, 1.0Å and 2500mm. CCD with image intensifier and Pilatus 2. We also performed in-house SAXS experiment with conventional small-angle. SAXS profiles were measured after attaining the equilibrium states. The obtained data was corrected for air scattering and electrical background. Then we obtained the 1D SAXS profiles by circularly averaging the 2D data.

Prior to TEM observation, the samples were microtomed into 100 nm thickness at -120°C and stained with OsO<sub>4</sub>. In TEM image, thus, the dark part corresponds to polyisoprene. Unstained samples have natural contrast between the poly(dimethylsiloxane) and the two other polystyrene/ polyisoprene domains due to the higher electron density of silicon unit. The TEM observation was performed using JEM-2000FX with the acceleration voltage being 200kV.

3D images of morphologies have been analyzed by electron tomography based on the computed tomography (CT). For dual-axis electron tomography, two orthogonal sets of TEM series images were taken from the ultrathin section specimen. Series of TEM images was acquired at angles tilting from  $-60^{\circ}$  to  $+60^{\circ}$  in  $2^{\circ}$  increments. These obtained TEM images were aligned with respect to the gold fiducial markers. Reconstruction of 3D morphology was obtained by using the filtered-back-projection (FBP) method with IMOD program. We used the software Analyze 10 to analyze the 3D images.

### 5-3. Results and Discussion

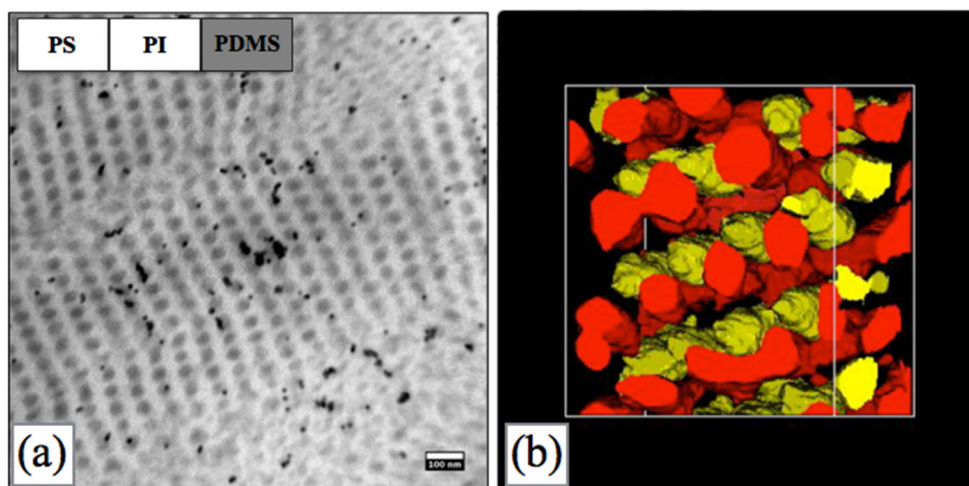
Figure 5-1 (a) shows the TEM image of PS-*b*-PI-*b*-PDMS (code: SID1) cast-film without staining. In the case of the unstained sample, the PDMS domain can be observed as dark phase due to the higher absorbing power of the Si atom. The dark PDMS domain exhibits six-fold symmetry in PS/PI domains, implying that PDMS domain seems to form hexagonally-packed cylinder structure. However, the stripe pattern of the side view of cylinder which is usually observed in TEM image of hexagonally-packed cylinders is not observed. The 3D image obtained by TEM-CT (Figure 5-1 (b)) allows us to notice that morphology is not a hexagonal-packed cylindrical structure, but two mutually interwoven, unconnected 3D networks of PDMS domain (red and yellow parts in Figure 5-1 (b)) embedded in the PS/PI matrix.

Figure 5-2 (a) shows a TEM image of the specimen stained with OsO<sub>4</sub>. The PI domains are stained darkly with OsO<sub>4</sub>, the less dark part corresponds to the PDMS domains, and the bright part corresponds to PS domains. PDMS domains are found in the PI domains as PI/PDMS core-shell structure and the core-shell structure PI/PDMS domains arranges hexagonally in PS matrix. It should be noted that the PS region forms the matrix of the double network structure even though the volume fraction of PS is 0.284 as the lowest in three components. In order to investigate the network structure in SID1 in details, we reconstructed 3D structure (Figure 5-2 (c)) of the selected region of TEM image (Figure 5-2 (b)).

Figure 5-2 (c) shows the reconstructed 3D image, the core-shell network

composed of PI and PDMS phases are indicated by red and yellow color, respectively, while the PS domain is the matrix or void. The analysis of the continuity of the region of PI/PDMS phases explored that PI/PDMS network structures consist of two independent networks. From the 3D reconstructed image, we can also confirm that this network structure exhibits six-membered-ring structural characteristics. In the OBDD phase, the minor component forms two interwoven periodic tetrapod-network, and the tetrapod-network structure forms a bicontinuous structure with a hexagonal symmetry, while the major component is the surrounding matrix. Therefore, we anticipate that the OBDD structure would be formed in SID1.

In order to characterize the network structure in detail, we shall focus on one of two independent networks. Figure 5-3 illustrates a series of clipped images of one network at various depths. At upper part in depth (Figure 5-3 (a)), branches directing upwards (marked by blue circles) are observed. In the middle part as shown in Figure 5-3 (b), six-membered rings can be observed and the branches are connected to alternate three nodes in the ring. At lower region (Figure 5-3 (c)), the branches directing downwards (marked by red circles) at another set of three nodes. From these three images, we can observe that the blue circles and the red circles in the images indicate nodes pointing upward and downward direction normal to the surface, respectively. According to the OBDD network model, branches at the six vertices in the six-membered ring arrange mutually directing side up and down of the plane as shown in Figure 5-4. The reconstructed 3D image of double network is consistent with the model of OBDD network as the spatial arrangements are the same.



**Figure 5-1.** (a) Electron micrograph of the SID1 cast film without staining, (b) Reconstruction 3D image of OBDD structure in SID1 without staining.

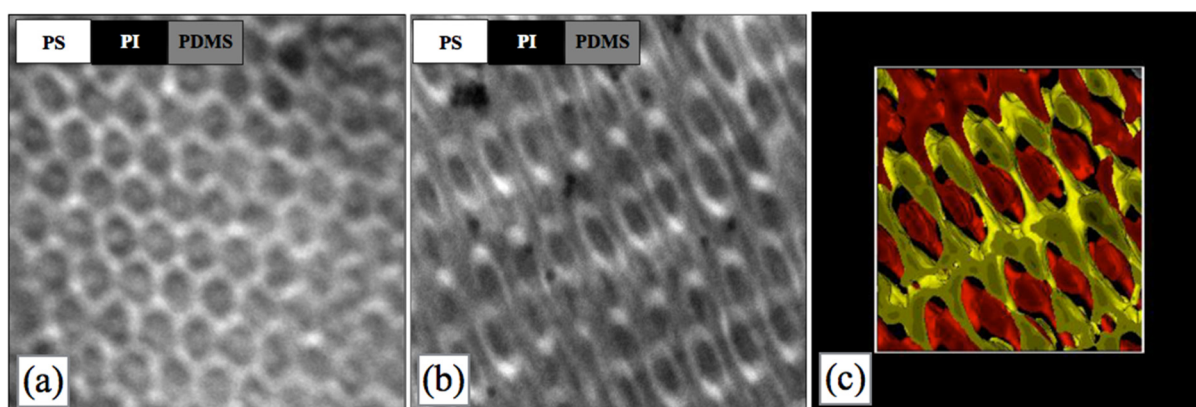


**Figure 5-2.** (a) (b) Electron micrograph of the SID1 cast-film stained with  $\text{OsO}_4$ , (c) Reconstruction 3D image of OBDD structure in SID1.

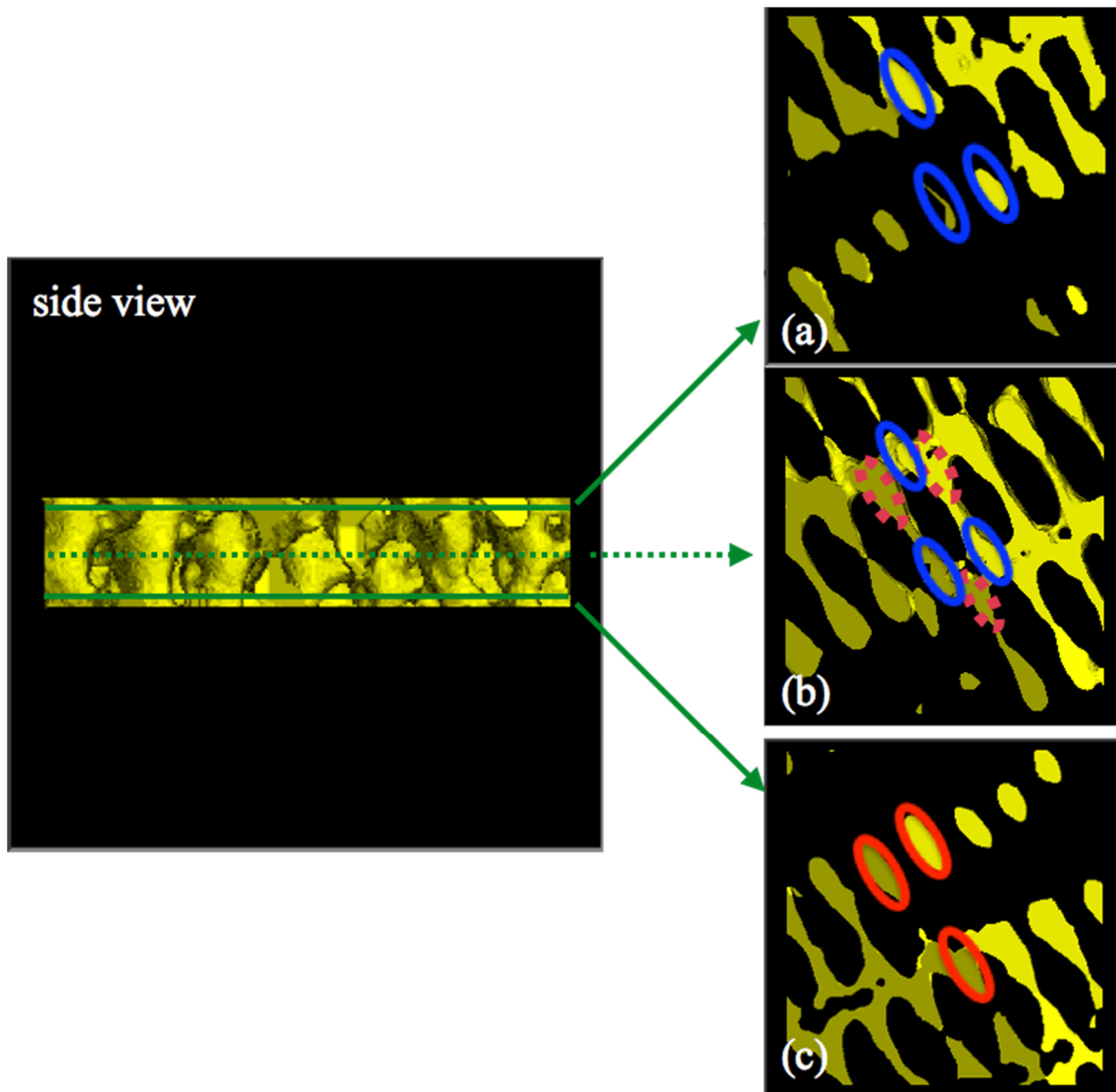


**Figure 5-3.** 3D clip images of isolated network of the double network structure. The blue circles and red circles in the image indicate nodes pointing normal to the surface with side up and side down direction, respectively. (a), (b) and (c) are slice image along corresponding region indicated in green line of side view.

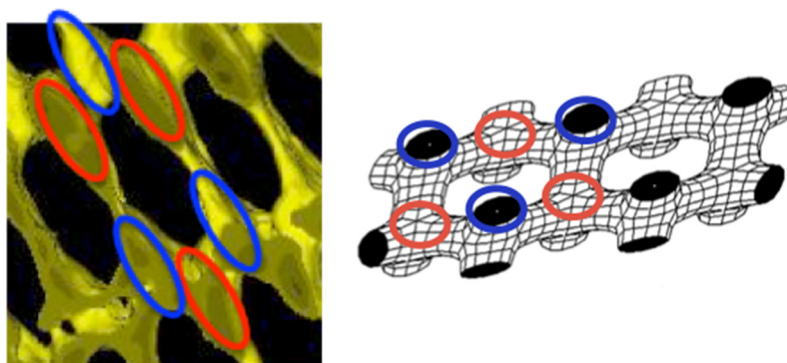


**Figure 5-4.** Comparison between the isolated network of reconstructed 3D image and the OBDD network structure model. Arrangement of the six vertices in the six-membered ring of TEM image and the OBDD model are the same: three vertices point side up direction (blue circles) of the plane and other three vertices point side down (red circles) of the plane.

OBDD structure determined by TEM was also confirmed by SAXS analysis.

Figure 5-5 (a) shows the SAXS profile of SID1 cast-film. The scattered intensity  $I(q)$  is plotted as a function of wave number  $q$  ( $q = (4\pi/\lambda)\sin(\theta/2)$ ;  $\theta$  is scattering angle and  $\lambda$  is wavelength of incident X-ray). The peaks at  $q/q_m = 1, \sqrt{3/2}, \sqrt{2}, \sqrt{3}$ , and 2 match up with the space group  $Pn3m$ , indicating double-diamond structure in the SID1 cast film. The TEM micrographs coupled with SAXS profile provide the evidence that SID1 self-assemble into OBDD structure during casting process.

After annealing at 130°C for 1 week, the morphology of SID1 transforms from OBDD to gyroid structure as indicated in Figure 5-5 (b), since SAXS profile has peaks located at  $q/q_m = 1, 1.15, 1.53, 1.8, 1.9$ , and 2, which agree with those calculated for the gyroid structure. Therefore, the equilibrium structure of SID1 should be the gyroid structure.

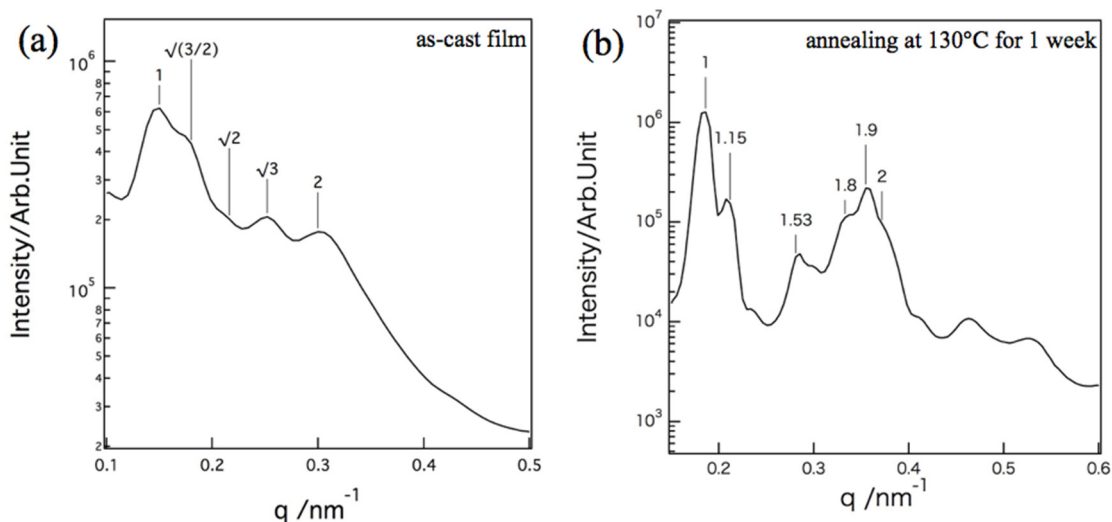


**Figure 5-5.** SAXS profiles for SID1 (a) cast-film and (b) after annealing at 130°C for 3 days.

In order to investigate the formation process of OBDD structure in SID1 during the solvent casting process, we measured SAXS of 30-50 wt % SID1 solutions. Figure 5-6 shows the concentration dependence of SID1 structure in SAXS profiles. We can observe the broad peak originating from the short range order of the micelle structures in solution at 30 wt%. At lower concentration (35 and 37 wt %), a scattering maxima at the scattering angles in the ratios of  $1: \sqrt{3}: \sqrt{4}: \sqrt{7}$  appears in the SAXS profiles. Hexagonally-packed cylindrical domain structures are usually found to have such behavior. In cast film, series lattice peaks of 1,  $\sqrt{3/2}$ ,  $\sqrt{2}$ ,  $\sqrt{3}$ , and  $\sqrt{4}$  shows a double-diamond structure with the space group  $Pn3m$ , indicating the hexagonally-packed cylindrical domain structures transformed into OBDD network structures.

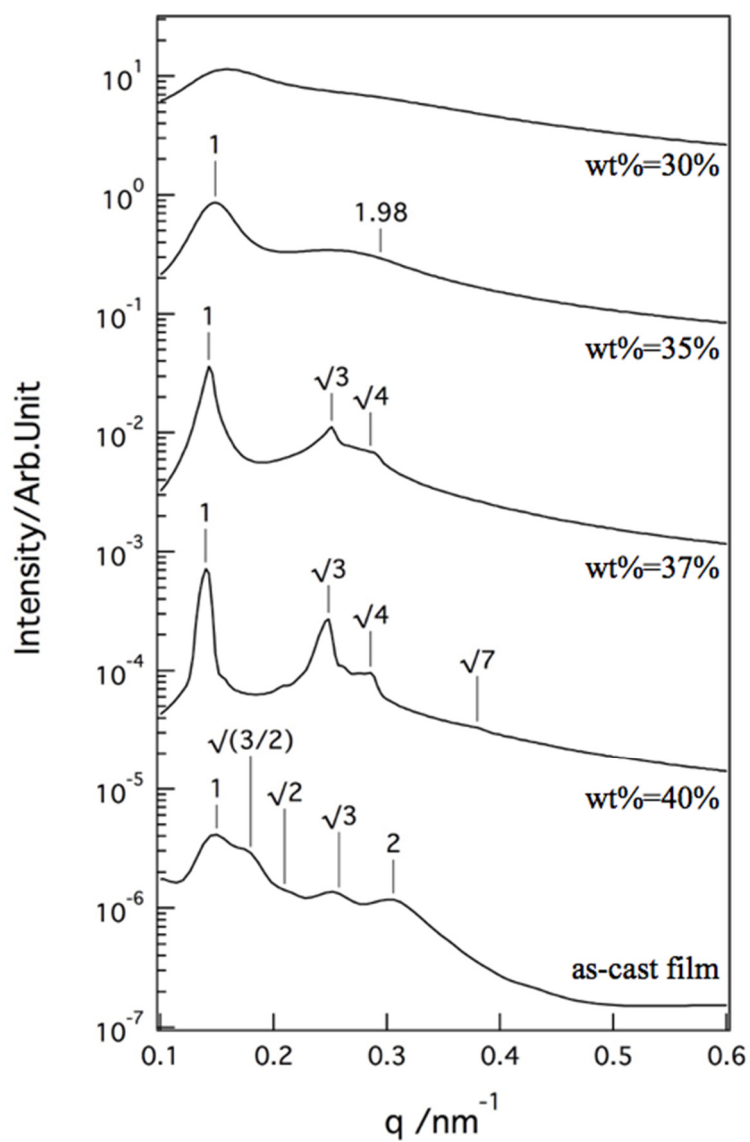


**Figure 5-6.** Concentration dependence of SAXS profiles for SID1 solution. The profiles are shifted vertically to avoid overlapping.

SAXS study has shown that the formation of OBDD structure is caused by a two-step microphase-separation as shown in Figure 5-7. In the solvent cast process, toluene used as solvents in cast process has a lower affinity towards PDMS chains in PS-*b*-PI-*b*-PDMS triblock copolymer. For PS and PI blocks, toluene is not a completely neutral solvent, but slightly selective towards PI. In the first step, as the result of segregation between PDMS chains and toluene, and the unfavorable enthalpic interaction between PS and PDMS (i.e., that  $\chi_{SD} > \chi_{ID} > \chi_{SI}^{19, 20}$ ), the microphase separation firstly occurs between PDMS and PS/PI and PDMS-cylinders are formed in PS/PI matrix. With increasing in concentration of polymer, segregation power between the remaining PS and PI components increases, and finally PS and PI segregate from each other within the pre-constructed microdomain formed in the first step of microphase-separation process. This two-step phase separation result in OBDD network structure during the self-assembly process of SID1 in solvent cast process.

We shall consider the reason why the transition from cylinder to OBDD occurs in this self-assembly process even though the OBDD is not the equilibrium morphology. Masten have studied the transition between cylinder and gyroid in diblock copolymer system after the onset of quench from cylinder phase to gyroid phase<sup>21</sup>. The transition is found to progress via nucleation and growth, and Masten predicted the topography of the Landau free energy surface of diblock copolymer to exhibit a pathway connecting the local minima of the cylinder and gyroid. Transformation of cylinder into gyroid starts from the fivefold coordinated junction as indicated by the arrows in the Figure 5-8 (a), which is evolved from subtle bulges of cylinders, and break

to leave as a threefold junction characteristic of gyroid. During this transition, a highly unfavorable two free ends (red circles in Figure 5-8 (a)) of the cylinder are formed and then quickly transform to two fourfold junction that would later break to produce threefold junction. Finally, cylinder transforms into gyroid as the above process repeats. We postulate that there is only one free end formed during the transition from cylinder to OBDD as indicated by red circle in Figure 5-8 (b). According to the composition of SID1, interface between PS and PI would curve towards PS domain since  $f_{PI} > f_{PS}$ , which makes it much more difficult for cylinders to form free ends during the evolution. Alternatively, cylinder may prefer to transform into one free end instead of two free ends in order to pass through a route with lower energy barriers. As a result, the structure with one free end evolves into fourfold junction representative of OBDD and OBDD structure grows during casting process though gyroid structure is identified to be an equilibrium structure in triblock copolymer systems. During the self-assembly process of SID triblock copolymer, formation of disconnection point in the intermediate process of evolution from cylinder is crucial and the energy barrier dominated the formation of the OBDD structure.

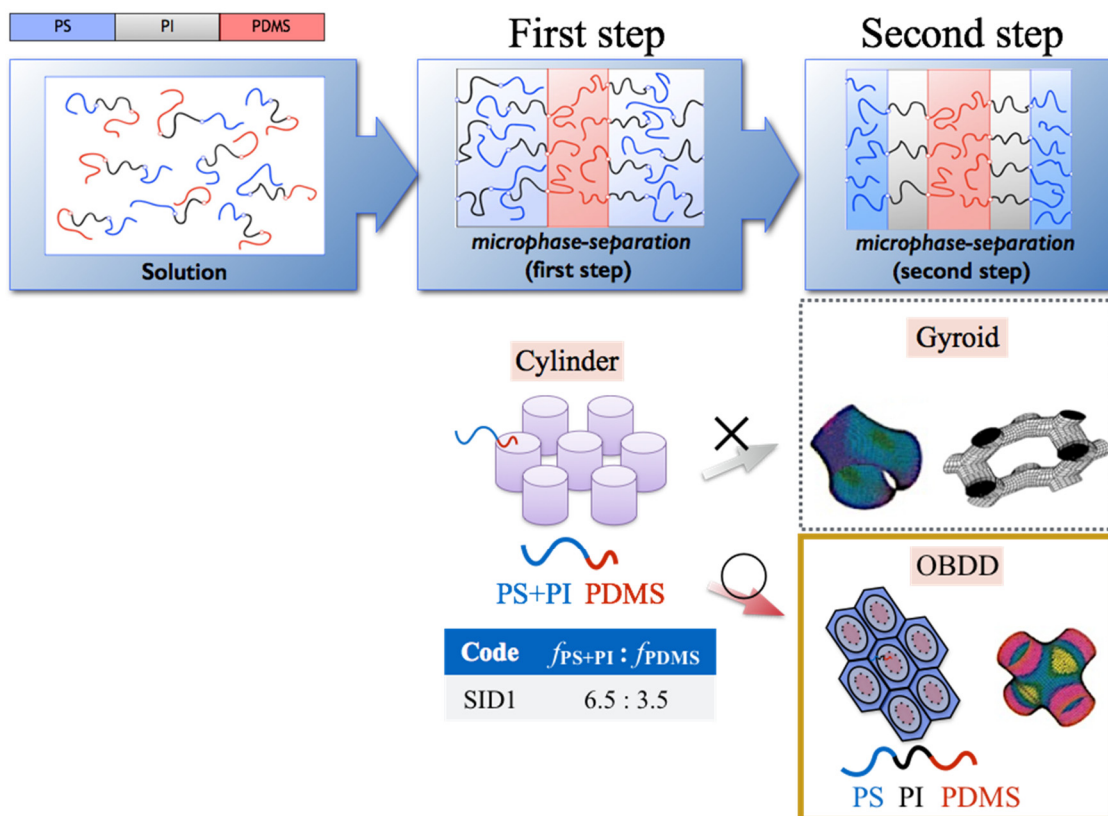


**Figure 5-7.** Scheme of two-step microphase separation during self-assembling process of SID1.

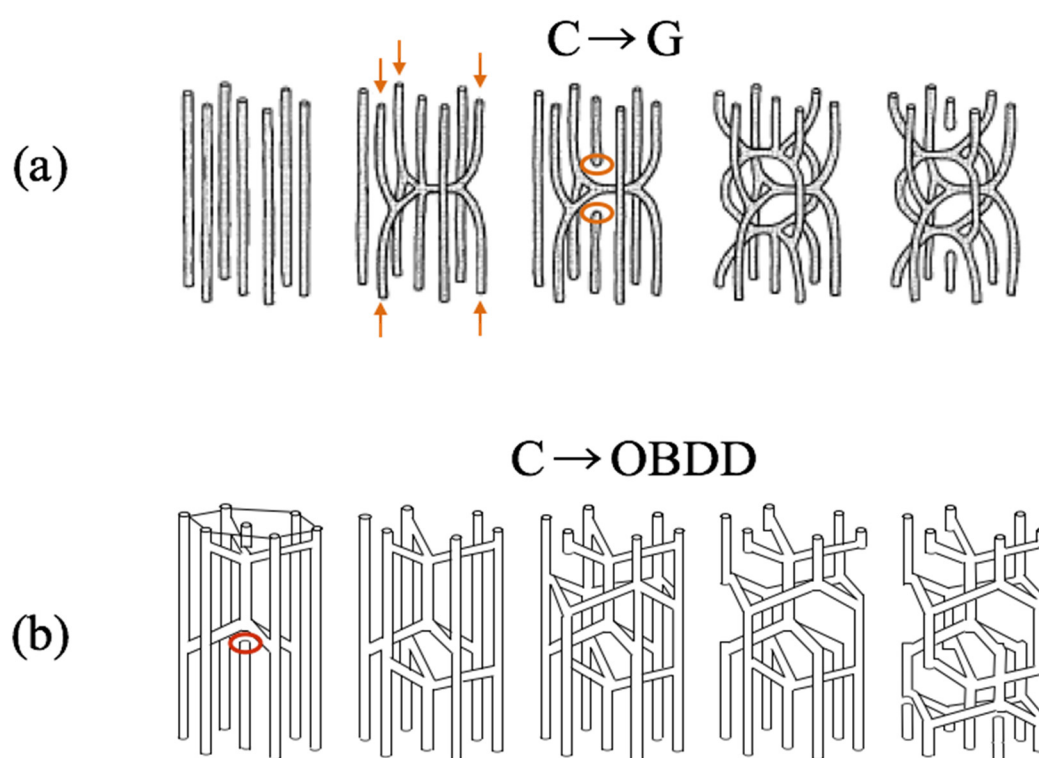


**Figure 5-8.** Schematic illustration of evolution of the minority domain for the (a)  $C \rightarrow G$  (top panels)<sup>21</sup> and (b)  $C \rightarrow OBDD$  (bottom panels) transitions.

## 5-4. Conclusions

We investigated the morphology of the SID1 triblock copolymer film cast from its toluene solution by TEM and SAXS. OBDD was found in the SID1 cast-film and the double network consisting of PDMS domains surrounded by PI are embedded in a PS matrix.

According to the SAXS result, formation of this bicontinuous OBDD network morphology is caused by a two-step microphase-separation. In the first step, PDMS segregates and packs hexagonally as PDMS-cylinders in PS/PI matrix. Then, due to the kinetics effect, PDMS-formed cylinders prefer to transform into OBDD structure through a one free end intermediate structure, which could reduce the energy barrier during rearrangement process of cylinder.

Among the SID1 casting process, relative magnitude of the different  $\chi$  parameters between PS, PI, and PDMS blocks and the kinetic barrier effect are significant. The pre-formed cylinders and the microstructural arrangement of SID1 result in the formation of the metastable OBDD network structure.

## Reference

1. Kudose, I.; Kotaka, T.; *Macromolecules* **1984**, 17, 2325-2332.
2. Mogi, Y.; Kotsuji, H.; Kaneko, Y.; Mori, K.; Matsushita, Y.; Noda, I. *Macromolecules* **1992**, 25, 5408-5411.
3. Stadler, R.; Auschra, C.; Beckmann, J.; Krappe, U.; Voigt-Martin, I.; Leibler, L. *Macromolecules* **1995**, 28, 3080-3097.
4. Zeng, W.; Wang, Z. G. *Macromolecules* **1995**, 28, 7215-7223.
5. Erukhimovich, I.; Abetz, V.; Stadler, R. *Macromolecules* **1997**, 30, 7435-7443.
6. Breiner, U.; Krappe, U.; Thomas, E. L.; Stadler, R. *Macromolecules* **1998**, 31, 135-141.
7. Shefelbine, T. A.; Vigild, M. E.; Matsen, M. W.; Hajduk, D. A.; Hillmyer, M. A.; Cussler, E. L.; Bates, F. S. *J. Am. Chem. Soc.* **1999**, 121, 8457-8465.
8. Bailey, T. S.; Pham, H. D.; Bates, F. S. *Macromolecules* **2001**, 34, 6994-7008.
9. Epps, T. H., III.; Cochran, E. W.; Hardy, C. M.; Bailey, T. S.; Waletzko, R. S.; Bates, F. S. *Macromolecules* **2004**, 37, 7085-7088.
10. Sugiyama, M.; Shefelbine, T. A.; Vigild, M. E.; Bates, F. S. *J. Phys. Chem. B* **2001**, 105, 12448-12460.
11. Bailey, T. S.; Hardy, C. M.; Epps, T. H.; Bates, F. S. *Macromolecules* **2002**, 35, 7007-7017.
12. Chatterjee, J.; Jain, S.; Bates, F. S. *Macromolecules* **2007**, 40, 2882-2896.
13. Cochran, E. W.; Bates, F. S. *Phys. Rev. Lett.* **2004**, 93, 087802/1- 087802/4.

14. Meuler, A. J.; Fleury, G.; Hillmyer, M. A.; Bates, F. S. *Macromolecules* **2008**, 41, 5809-5817.
15. Matsushita, Y.; Suzuki, J.; Seki, M. *Physica B: Condensed Matter* **1998**, 248, 238-242.
16. Matsushita, Y.; Torikai, N.; Suzuki, J.; Seki, M. *J. Phys. Chem. Solids* **1999**, 60, 1279-1284.
17. Seki, M.; Suzuki, J.; Matsushita, Y. *J. Appl. Crystallogr.* **2000**, 33, 285-290.
18. Suzuki, J.; Seki, M.; Matsushita, Y. *J. Chem. Phys.* **2000**, 112, 4862-4868.
19. Hashimoto, T.; Ijichi, Y.; Fetters, L. J. *J. Chem. Phys.* **1988**, 89, 2463-2472.
20.  $\chi_{ID} = 43.6/T - 0.010$ ,  $\chi_{SD} = 68/T + 0.037$ , measured by Kristoffer ALmdal.
21. Masten, M. W. *Phys. Rev. Lett.* **1998**, 80, 4470-4473.



## ***Chapter 6***

# **Morphological Control in PS-*b*-PI-*b*-PDMS Triblock Copolymer by Mixed-Solvent**

### **6-1. Introduction**

Various kinds of periodic morphologies have been extensively studied over decades<sup>1-6</sup>. In addition, several researches have put emphasis toward complex systems, such as multiblock copolymers and non-linear block copolymers<sup>7-10</sup>, and broaden the extent that various microdomain morphologies and different microdomain sizes can be accessed. In equilibrium state of strong segregation limit, the morphologies of block copolymers depend on only volume fraction of each constituent polymer and their architectures, and the synthesis processes are very important to control their morphologies.

In previous work, we have, however, shown that the ordered bicontinuous double-diamond morphology (OBDD) made from slightly asymmetric linear polystyrene-*block*-polyisoprene-*block*-polydimethylsiloxane (code: SID1) triblock copolymer ( $f_{PS} = 0.284$ ,  $f_{PI} = 0.36$ ,  $f_{PDMS} = 0.356$ ) cast from toluene solution, even though OBDD is not an equilibrium structure of triblock copolymers. Among the solvent cast process, two-step phase separation occurred due to the selectivity of solvent and resulted in an OBDD network structure during the self-assembly process of SID1 triblock copolymer. This indicates that the selectivity of solvent can induce non-equilibrium structure by using solvent-cast method. In the case of polystyrene-*block*-polyisoprene (SI) diblock copolymer, cylinder structure can be induced in symmetric SI diblock copolymer, which usually forms LAM, by solvent cast with selective solvent for PS. The cylinder structure is induced by the increase of effective volume fraction of PS with selective solvent, and then the vitrification of PS freezes the non-equilibrium structure.

In this study, we demonstrated the tunability of the microdomain morphology in polystyrene-*block*-polyisoprene-*block*-polydimethylsiloxane (code: SID2) triblock copolymer produced from its solution using mixed-solvent of toluene and n-decane. By varying the weight ratio of toluene/n-decane in the mixed-solvent, ordered microdomain morphologies such as spheres, hexagonally-packed cylinders, lamellae and OBDD network structure could be formed in the polymer solution. Moreover, ordered microdomain morphologies found in the solution can be preserved in the bulk state.

## 6-2. Experimental Section

Polystyrene-*block*-polyisoprene-*block*-polydimethylsiloxane (code: SID2) was synthesized via living anionic polymerization in benzene under an argon environment using *sec*-BuLi as an initiator. Number-average molecular weight ( $M_n$ ) and polydispersity index (PDI) of SID2 triblock copolymer was determined by gel permeation chromatography (GPC) using polystyrene standards. For GPC measurement, THF was used as the eluent at 40°C. Volume fraction of polystyrene, polyisoprene and polydimethylsiloxane ( $f_{PS}$ ,  $f_{PI}$  and  $f_{PDMS}$ ) were determined by using  $^1\text{H}$  nuclear magnetic resonance (NMR) spectroscopy. The characterizations of the samples are listed in Table 6-1.

The cast film of SID2 was obtained from the 10 wt% toluene solution of SID2 polymer after casting for 1 week, and we characterized the structure of cast film by SAXS and TEM. To confirm the equilibrium structure of SID2 in bulk, we annealed the cast film of SID2 at 130°C for 1 week. The annealed sample was measured with SAXS.

In order to control the morphologies by using mixed-solvent, we employed toluene and *n*-decane. Table 6-2 lists the solubility parameters of the solvents and the constituent polymers. Toluene is selective to PS and PI while *n*-decane is selective to PDMS. Four SID2 polymer solutions with different weight mixing ratio (1/2, 1/1.5, 1/1.3, 1/1.2) of toluene/*n*-decane were prepared. The microdomain structures of SID2 triblock copolymers in the solution and in the bulk films cast from the corresponding solution were observed by SAXS.

Prior to TEM observation, the samples were microtomed into 100 nm thickness at  $-120^{\circ}\text{C}$  and stained with  $\text{OsO}_4$ . In TEM image, thus, the dark part corresponds to polyisoprene. Unstained samples have natural contrast between the poly(dimethylsiloxane) and the two other polystyrene/ polyisoprene domains due to the higher electron density of silicon unit. The TEM observation has been performed using JEM-2000FX with the acceleration voltage being 200kV.

Synchrotron SAXS experiments were performed at BL45XU in SPring-8 to examine the morphologies of the cast film and the solution. At BL45XU, the wavelength and the sample-to-detector distance are, respectively,  $1.0 \text{ \AA}$  and 2500mm. CCD with image intensifier and Pilatus with pixel array detector were used as a detector. The obtained data was corrected for air scattering and electrical background. Then we obtained the 1D SAXS profiles by circularly averaging the 2D data.

**Table 6-1.** Molecular Characteristics of SID2 Triblock Copolymer.

Code	$M_n (\times 10^4)(g \cdot mol^{-1})$	$f_{PS}$	$f_{PI}$	$f_{PDMS}$	$M_w/M_n$
SID2	3.24	0.29	0.43	0.28	1.05

**Table 6-2.** Solubility Parameters of the Polymers and Solvents Investigated.

Material	Solubility Parameter ( $MPa^{1/2}$ )
PS	8.5-10.3
PI	8.13
PDMS	7
Toluene	8.8
n-decane	7.74

## 6-3. Results and Discussion

### 6-3-1. Equilibrium Structure of SID2 Triblock Copolymer

Firstly, we checked the equilibrium structure formed in the SID2. Figure 6-1 shows the SAXS profile of SID2 cast film after annealing at 130°C for 1 week. The scattered intensity  $I(q)$  is plotted as a function of wave number  $q$  ( $q = (4\pi/\lambda)\sin(\theta/2)$ ;  $\theta$  is scattering angle and  $\lambda$  is wavelength of incident X-ray). The peaks at  $q/q_m = 1, 1.15, 1.53, 1.83, 1.93,$  and  $2$  match up with the space group  $Pn3m$ , indicating the gyroid structure is formed in the SID2 cast film. Therefore, the equilibrium structure of SID2 should be the gyroid structure.

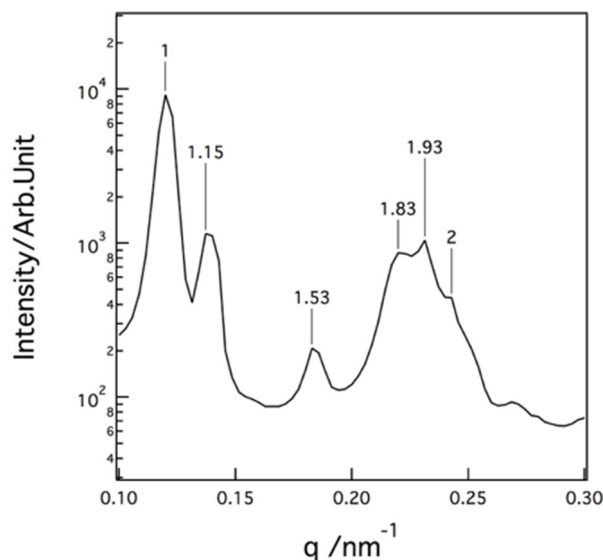


**Figure 6-1.** SAXS profiles for SID2 after annealing at 130°C for 1 week.

### 6-3-2. Morphology of SID2 Film Cast from Toluene Solution

The microdomain structure in the SID2 film cast from the toluene solution was examined via TEM. Figure 6-2 (a) shows the TEM image of SID2 triblock copolymer cast film without staining. The PDMS domain is dark and exhibits six-fold symmetry in the white PS/PI domains in the unstained sample, indicating that PDMS domain seems to form hexagonally-packed cylindrical structure. However, the stripe pattern of the side view of cylinder is not observed. Figure 6-2 (b) shows a TEM image of the specimen stained with OsO<sub>4</sub>. In this case, the PI domains are dark, the less dark layer corresponds to the PDMS domains, and the bright layer corresponds to PS domains. PDMS domains are found in the PI domains as PDMS/PI core-shell structure and packs hexagonally in PS matrix. The similar morphology was also observed in the SID1 cast film in the previous chapter. Compared the TEM images with that of the previous results of OBDD-forming SID1, the six-membered ring structure and the similar bicontinuous network structure are observed in both SID1 and SID2 films, indicating that the OBDD structure is also formed in the SID2 film. It should be noted that the OBDD is a metastable structure, and the equilibrium structure of SID2 should be the gyroid structure.

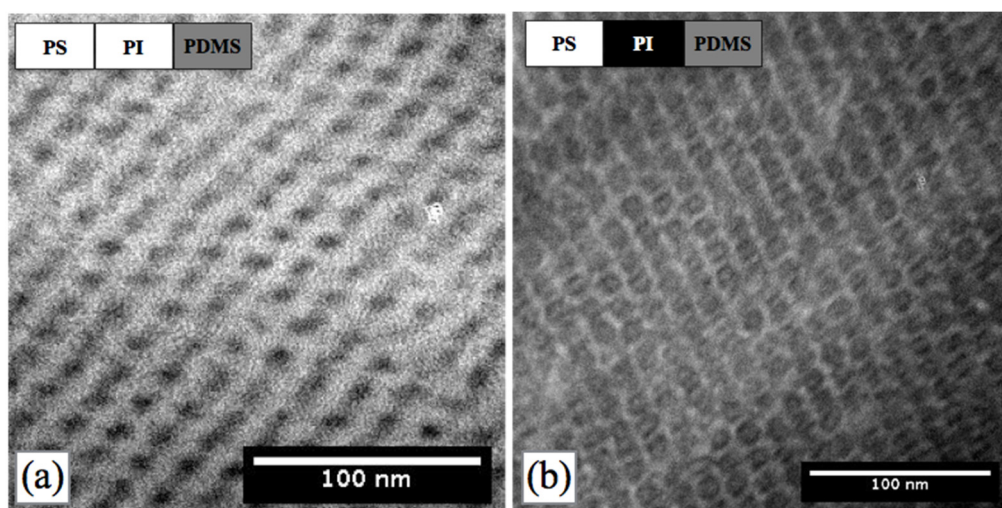


**Figure 6-2.** Electron micrograph of the SID2 cast film (a) without staining, (b) stained with OsO<sub>4</sub>.

### 6-3-3. Morphology of SID2 Solutions with Different Weight Ratio in Mixed-Solvent

The effects of different ratio between toluene and n-decane solvents on the microphase separation microdomain structures of SID2 triblock copolymer are demonstrated. Toluene prefers to stay in the PS phase while n-decane goes less into PS phase and more to the PI and PDMS phase. Figure 6-3 shows the mixed-solvent ratio dependence of SAXS profiles of different SID2 polymer solutions. When n-decane is twice of the weight of the toluene in the mixed-solvent, the solution has a spherical microdomain morphology as the peaks at  $q/q_m = 1, \sqrt{2}, \sqrt{3}, \sqrt{4}, \sqrt{5}, \sqrt{6}, \sqrt{7},$  and  $\sqrt{9}$  are found in the SAXS profiles, these peak positions indicate that the spherical structure was formed. When the weight ratio of toluene and n-decane is 1:1.5, the ratios of  $q/q_m$  become different from those of the spherical structure. SAXS peaks are located at  $q/q_m = 1, \sqrt{3}, \sqrt{4}, \sqrt{7},$  and  $\sqrt{9}$ , agreeing with the peak ratio of the hexagonally-packed cylinder structure. As the ratio between toluene and n-decane gradually decreases to 1:1.3, distinct peak position ratio at 1, 2, 3, 4, 5, and 6 indicates lamellar structure is formed. OBDD network structure is formed when the ratio between toluene and n-decane is 1:1.12 since the SAXS profile has peaks located at  $q/q_m = 1, \sqrt{(3/2)}, \sqrt{(5/2)}, \sqrt{3},$  and 2.

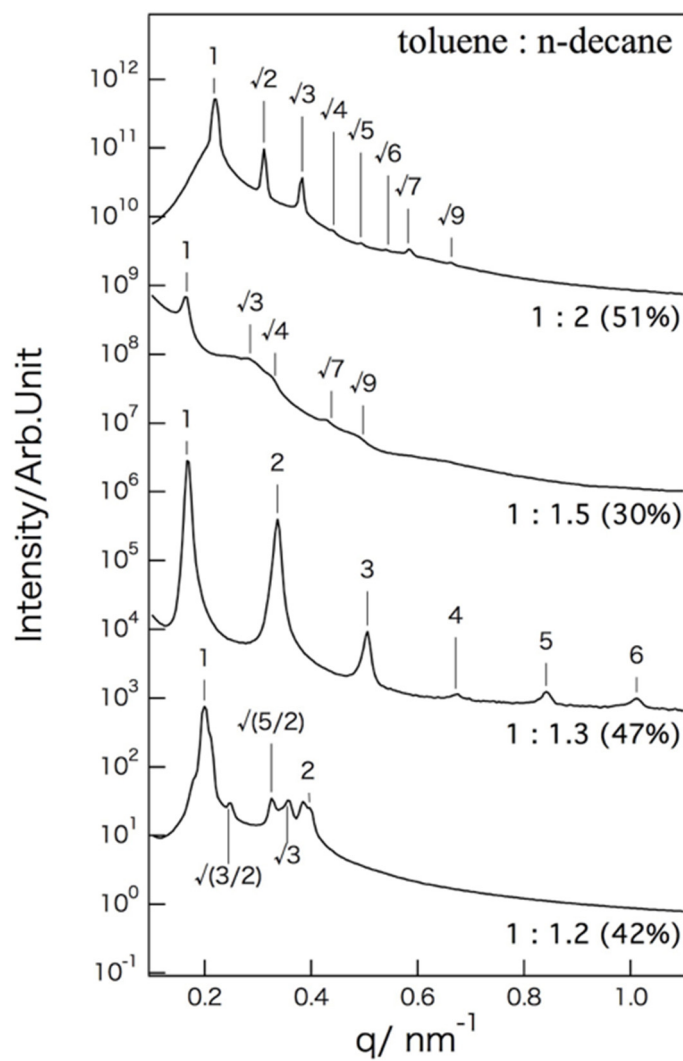


**Figure 6-3.** SAXS profiles of different weight ratio between toluene/n-decane for SID2 solution. The profiles are shifted vertically to avoid overlapping.

### 6-3-4. Preservation of Morphologies of Solution State

The SAXS profiles of SID2 in 30 wt% solution with mixing ratio at 1/1.5 (toluene/n-decane) and in bulk film cast from the solution are shown in Figure 6-4 (a) and 6-4 (b), respectively. As mentioned above, at this mixing ratio, the microdomain structure exhibits hexagonally-packed cylinders. After casting from the mixed-solvent, the peaks at  $q/q_m = 1, \sqrt{3}, \sqrt{4}, \sqrt{7},$  and  $\sqrt{9}$  are observed, indicating that the microdomain structure, hexagonally-packed cylinders, is preserved in bulk state.

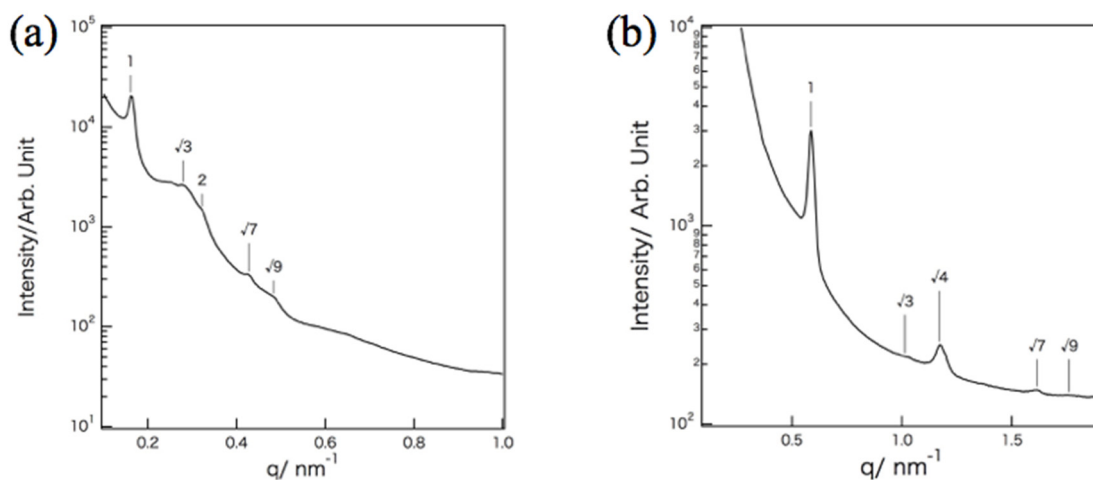


**Figure 6-4.** SAXS profiles of (a) 30 wt% SID2 1/1.5 with toluene/n-decane mixed-solvent solution profile and (b) bulk film cast from the mixed-solvent solution.

The SAXS profiles of SID2 in 47 wt% mixed-solvent solution with mixing ratio at 1/1.3 (toluene/n-decane) and in bulk film cast from the solution are shown in Figure 6-5 (a) and 6-5 (b), respectively. At this mixing ratio of 1/1.3 between toluene and n-decane, the lamellar microdomain structure is formed in the solution. After casting from the solvent, the peaks located at  $q/q_m = 1, 2, 3,$  and  $5$  are observed, indicating that the lamellar microdomain structure is preserved in bulk state.

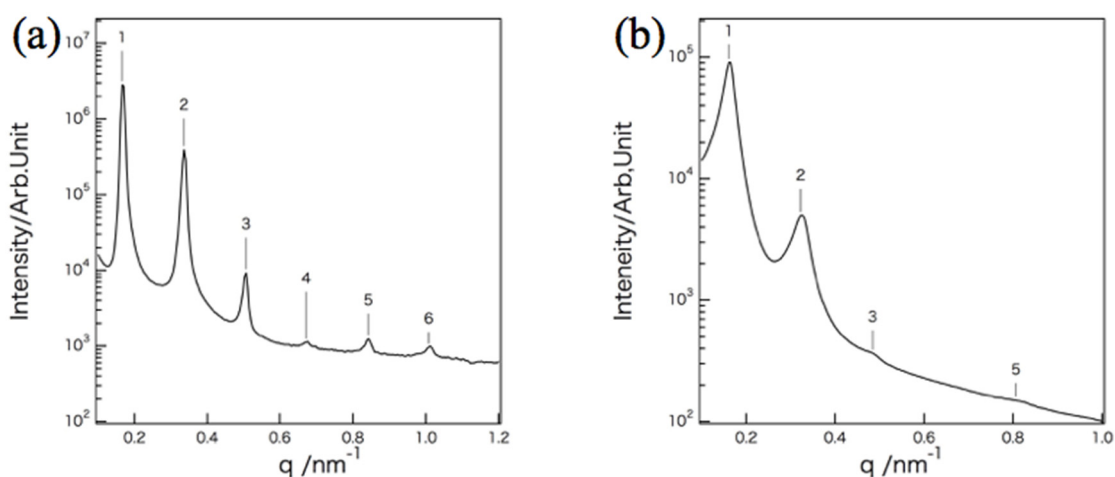


**Figure 6-5.** SAXS profiles of (a) 30 wt% SID2 with 1/1.3 toluene/n-decane mixed-solvent solution profile and (b) bulk film cast from the mixed-solvent solution.

## 6-4. Conclusions

We revealed interesting features of the phase behaviors of SID2 triblock copolymer having gyroid structure in its equilibrium state by applying mixed toluene/n-decane solvents. Starting from pure toluene cast film, OBDD structure is first found as the ordered structure in SID2 triblock copolymer. The progressive addition of n-decane into toluene is found to induce a morphological transition, and various ordered microdomain structures are formed. Based on the SAXS result, at the mixing weight ratio of 1/2 toluene/n-decane, the micro-separated structure is spheres in BCC lattice. The hexagonally-packed cylinder is observed as the mixing ratio is 1/1.5 toluene/n-decane. Lamellar structure can be obtained if the mixing ratio between toluene and n-decane is 1/1.3. For the 1/1.2 toluene/n-decane weight ratio being, which is the most similar to that of pure toluene used in casting process, the SAXS profile shows the identical OBDD structure as observed in toluene-cast film. Furthermore, the hexagonally-packed cylinders and the lamellae are persisted in the bulk film cast from the corresponding solutions, indicating the morphologies formed in the solution can be preserved in the bulk state. According to the results, mixed-solvent can be used as a key technique for controlling and creating a variety of ordered microdomain structures in SID triblock copolymers.

## Reference

1. Matsen, M. W.; Schick, M. *Phys. Rev. Lett.* **1994**, 72, 16, 2660-2663.
2. Matsen, M. W.; Bates, F. S. *Macromolecules* **1996**, 29, 4, 1091-1098.
3. Mani, S.; Weiss, R. A.; Cantino, M. E.; Khairallah, L. H.; Hahn, S. F.; Williams, C. E. *European Polymer Journal* **2000**, 36, 1, 215-219.
4. Huckstadt, H.; Goldacker, T.; Gopfert, A.; Abetz, V. *Macromolecules* **2000**, 33, 10, 3757-3761.
5. Huckstadt, H.; Gopfert, A.; Abetz, V. *Polymer* **2000**, 41, 26, 9089-9094.
6. Seki, M.; Suzuki, J.; Matsushita, Y. *J. Appl. Crystallogr.* **2000**, 33, 285-290.
7. Stadler, R.; Auschra, C.; Bechmann, J.; Krappe, U.; Voigtmartin, I.; Leibler, L. *Macromolecules* **1995**, 28, 3080-3097.
8. Wei, Z.; Wang, Z. G. *Macromolecules* **1995**, 28, 7215-7223.
9. Matsen, M. W. *J. Chem. Phys.* **1998**, 108, 785-796.
10. Matsen, M. W.; Schick, M. *Macromolecules* **1994**, 27, 4014-4015.

## Summary

In this thesis, I focused on the control of the complex network microdomain morphologies by different methods such as (i) composition control by synthesis, and by adding homopolymer into neat diblock copolymer; (ii) architectural design of block-graft copolymer; (iii) two-step microphase separation, and (iv) cast method with mixed-solvent. The network microdomain morphologies were investigated by SAXS and TEM.

In Chapter 2, the *Fddd* phase in polystyrene (PS) rich region or  $f_{PI} < 0.5$  of the phase diagram for polystyrene-*block*-polyisoprene (SI) diblock copolymers was investigated by using SAXS and TEM, where  $f_{PI}$  is a volume fraction of polyisoprene (PI) in SI diblock copolymer. We found the *Fddd* phase as an equilibrium phase in the range of  $0.37 \leq f_{PI} \leq 0.373$  and  $19.5 < \chi N < 21.1$ . The *Fddd* phase boundary in PS-rich region is much narrower than that in PI-rich region or  $f_{PI} > 0.5$  in terms of  $f_{PI}$ , and  $\chi N$ . The asymmetry of *Fddd* regime between PS-rich and PI-rich region can be explained by the conformational asymmetry between PS and PI chains.

In Chapter 3, the *Fddd* structure was found in polystyrene-*block*-polyisoprene (SI) diblock copolymer which does not have *Fddd* phase by adding polystyrene (hPS) homopolymer. The SI/ hPS blend samples were prepared in the range of  $0.627 < f_{PI} < 0.646$  and we investigated the phase boundary of *Fddd* phase by using SAXS and TEM,

where  $f_{PI}$  is volume fraction of polyisoprene (PI) in SI/ hPS. The *Fddd* phase was found as an equilibrium phase in the range of  $0.632 \leq f_{PI} \leq 0.641$  and  $27.5 < \chi N < 30.2$ . The *Fddd* phase boundary in the SI/ hPS is similar to that in the neat SI block copolymer since the hPS with the low molecular weight does not change the critical point  $(\chi N)_C$  for the microphase separation of the blends.

In Chapter 4, OBDD morphology was found in polystyrene-*block*-(poly-4-vinylphenyldimethylvinylsilane-*graft*-polyisoprene), PS-*b*-(PVPDVS-*g*-PI), block-*graft* copolymer. Via electron microscopy of PS-*b*-(PVPDVS-*g*-PI), it is identified that the constituting unit is a tetrapod comprising of four rodlike segments of major PS phase. These tetrapod units connect together as a planar six-membered ring and for an ordered three-dimensional OBDD network and the minor PI fills up the matrix phase. The packing frustration of *graft* chain is relaxed by the broad distribution of the curvature in OBDD network structure. The architecture of PS-*b*-(PVPDVS-*g*-PI) block-*graft* copolymer is responsible for the inverse of the OBDD network structure.

In Chapter 5, OBDD was formed in film of polystyrene-*block*-polyisoprene-*block*-polydimethylsiloxane (code: SID1) triblock copolymer cast from toluene solution, though OBDD structure is not an equilibrium structure in triblock copolymers. The SAXS study explored that the following two-step microphase separation proceeded during solvent cast: In the early stage of the cast process, hexagonally-packed polydimethylsiloxane (PDMS) cylinders were self-assembled in polystyrene (PS)/ polyisoprene (PI) matrix where PS and PI in

disordered state. Subsequently, order-order transition then was induced by microphase separation between PS and PI with the increase of concentration. Since the kinetic barrier of transition induced by the microphase separation between PS and PI from cylinder to gyroid is higher than that from cylinder to OBDD, the metastable OBDD was formed.

In Chapter 6, we have succeeded in controlling the morphology of polystyrene-*block*-polyisoprene-*block*-polydimethylsiloxane (code: SID2) triblock copolymer by solvent cast method with mixed-solvent of toluene and n-decane. As increase in the ratio of toluene, sphere, hexagonally-packed cylinder, lamellae, and OBDD network structure were found in the SID polymer solutions. Furthermore, bulk films cast from solutions showed the identical microdomain structures with those observed in the corresponding solutions. This study provides a new technique to control microphase-separated structures in triblock copolymers in solution and bulk state.



## List of Publications

1. “*Fddd* Phase Boundary of Polystyrene-*block*-polyisoprene Diblock Copolymer Melts in the Polystyrene-Rich Region”  
Wang, Y. C.; Matsuda, K.; Kim, M. I.; Miyosh, A.; Akasaka, S.; Nishitsuji, S.; Saijo, K.; Hasegawa, H.; Ito, K.; Hikima, T.; Takenaka, M.  
*Macromolecules* **2015**, 48 (7), 2211–2216.  
(Chapter 2)
2. “*Fddd* structure in Polystyrene-*block*-polyisoprene Diblock Copolymer/polystyrene Homopolymer Blends”  
Submitted to *Macromolecules*  
(Chapter 3)
3. “3D-TEM study on the Morphology of PS-*b*-(PVPDVS-*g*-PI) Block-Graft Copolymer”  
Submitted to *Macromolecules*  
(Chapter 4)

4. “The formation of OBDD Network Structure in PS-*b*-PI-*b*-PDMS Triblock Copolymer”  
Submitted to *Macromolecules*  
(Chapter 5)
  
5. “Morphological Control in PS-*b*-PI-*b*-PDMS Triblock Copolymer by Mixed-Solvent”  
Submitted to *Macromolecules*  
(Chapter 6)
  
6. “Visualizing patterned thin films by grazing-incidence small-angle X-ray scattering coupled with computed tomography”  
Ogawa, H.; Nishikawa, Y.; Fujiwara, A.; Takenaka, M.; Wang, Y. C.; Kanaya, T.; Takata, M.  
*Journal of Applied Crystallography* **2015**, 48, 1645-1650  
(Not included in this thesis)

## Acknowledgements

The present thesis is based upon the study carried out under the supervision of Professor Mikihito Takenaka, at the Department of Polymer Chemistry, Graduate School of Engineering, Kyoto University, from 2013 to 2016.

I would like to express my warmest appreciation to Professor Mikihito Takenaka for his continuous encouragement, guidance, valuable discussions, and patience throughout the research and the dissertation. I would also like to extend my sincere gratitude to Professor Hirokazu Hasegawa and Dr. Kenji Saijo for their encouragement and valuable comments in the course of the study.

Thanks are also due to the research group and for those who took a part in experimental, helpful technical, and collaboration especially regarding the entitled research. I would also like to thank to secretary of Takenaka Laboratory, Ms. Oda Naoka, for the kind care and helps for my life in Japan.

I would like to express my sincere gratitude to Japan Government in funding the Kouryuukyokai Scholarship (交流協会奨学金) which enabled me to undergo and complete a PhD program at the Kyoto University.

Finally, special thanks to my parents, my friends and Professor Hsin-Lung Chen for their love and care. Thanks for believing in me and the unlimited supports during my study.

December 2015

Yi-Chin Wang